Determining the geothermal potential of natural gas fields in the Southern North Sea

JEFFERIES, ALEXANDER,JAMES,PATRICK

Determining the geothermal potential of natural gas fields in the Southern North Sea

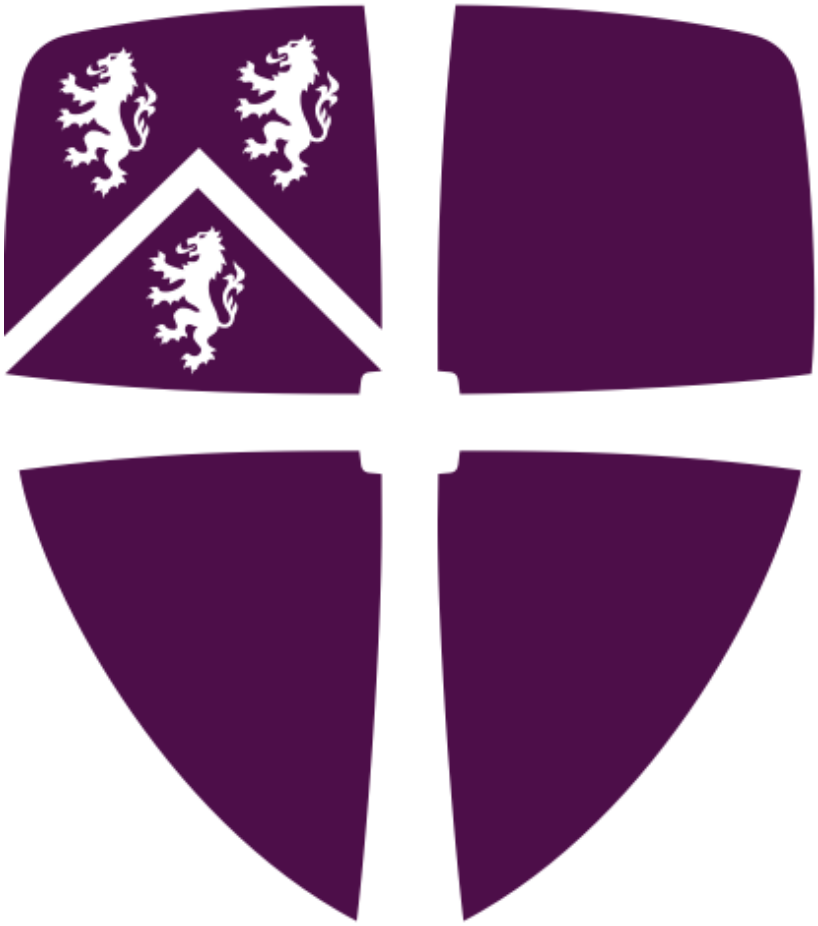

Alexander Jefferies

This thesis is submitted in partial fulfilment of the requirements for the degree of Master of Science by Research

Supervisors:

Prof. Jon Gluyas and Neil Fowler*

Department of Earth Sciences, Durham University

***Shift Geothermal Ltd**

Abstract

Renewable energy uptake must increase to reduce carbon emissions and curb today's unprecedented rate of global warming. CO_2-based geothermal energy extraction could be used to produce near zero-carbon power from the heat stored in depleted natural gas reservoirs. CO_2-plume geothermal (CPG) is a conceptual technology designed to produce power by circulating CO_2 through permeable and porous formations sealed by low-permeability cap rocks, ultimately storing industrial quantities of CO_2 in the subsurface. Few feasibility studies have considered the application of this technology to wide-scale geographical areas and no offshore CPG prospects have been evaluated. Several factors make natural gas fields in the Southern North Sea (SNS) promising CPG prospects; geothermal gradients are higher on average than those found onshore in the UK, infrastructure is already in place, extensive geological data are available, and seawater can be used as a heat sink to improve CPG performance. In this research, CPG power production is estimated for 64 SNS gas fields using a few identified and simplifying assumptions.

The South Sean field was selected as the field best suited for CPG in terms of power production potential and practicality. Power production was re-estimated for South Sean with increased accuracy. The gas fields are classified as geothermal resources following the United Nations Framework Classification for Resources (UNFC). Findings indicate that moderate amounts of power (in the order of kilowatts electric) could be produced from 50 of the 64 fields. An injection-production well doublet configured to South Sean could produce from 59 kWe to 552 kWe depending on well diameter sizing. This research demonstrates that low parasitic cooling loads can be achieved using seawater as a cooling medium, giving offshore CPG systems an edge over their onshore counterparts. All fields are classified under the UNFC system as having additional quantities in place, highlighting the need for a follow-up economic analysis.

Contents

List of figures

List of tables

Nomenclature

A	Surface area (m^2)
b	Gross reservoir thickness (m)
D	Well diameter (m)
f	Friction factor (dim)
g	Gravitational acceleration constant (m/s^2)
h	Specific enthalpy (kJ/kg)
k	Permeability (mD)
L	Well spacing (m)
$\dot{m}$	Mass flow rate (Kg/s)
$\dot{P}$	Power (kW)
P	Pressure (MPa)
Qc	Heat transfer rate into cold reservoir (W_{th})
Qh	Heat transfer rate out of hot reservoir (W_{th})
s	Specific entropy (kJ/(kg k))
Tc	Cold reservoir temperature (°C)
Th	Hot reservoir temperature (°C)
T_{ci}	Heat exchanger inlet temperature (H_2O) (°C)
T_{co}	Heat exchanger outlet temperature (H_2O) (°C)
T_{hi}	Heat exchanger inlet temperature (CO_2) (°C)
T_{ho}	Heat exchanger outlet temperature (CO_2) (°C)
U	Heat transfer coefficient ($W/m^2 \cdot K$)
W	Work (kJ)
z	Depth (m)
ΔT_{lm}	Logarithmic mean temperature difference (°C)
η	Efficiency
μ	Dynamic viscosity (Pa S)
ρ	Density (kg/m^3)

Acknowledgments

Foremost, I'd like to express my gratitude to my supervisors, Prof. Jon Gluyas and Neil Fowler. Jon's knowledge, patience, and understanding make him a brilliant mentor and role-model. Neil's expertise has also proven invaluable towards the completion of this research; our meetings encouraged me to focus on the details that matter most. My sincere thanks extend towards my family and friends for their constant love and support along the way.

1. Introduction

1.1 Aim and objectives

The aim of this thesis is to assess the geothermal potential of depleted natural gas fields in the Southern North Sea by estimating the electrical power that could be produced by direct CO_2-plume geothermal (CPG). The following objectives are set to achieve this aim:

- Develop a method for evaluating offshore CPG prospects
- Estimate CPG power production for each gas field on a macro-scale
- Select the most suitable gas field for CPG and re-estimate power production using a higher-resolution approach
- Report the estimations and classify the gas fields as geothermal resources in a standardised way

1.2 Global warming, renewables, and CCS

Ice core data has revealed strong evidence of past carbon dioxide levels (Friedli et al., 1986) (MacFarling Meure et al., 2006). CO_2 emissions accumulated worldwide from 1990 to present have now surpassed all emissions preceding 1990 - where drastic increases occurred on account of the industrial revolution (IPCC 2018). Since this time, two Kyoto protocol commitment periods have run their courses, and the Paris agreement has been established. Despite this, global atmospheric CO_2 continues to rise substantially. In 2020, 83% of global primary energy consumption was on account of using fossil fuels (BP plc, 2021). Renewable energy uptake must increase to help slow today's unprecedented rate of global warming and avoid potentially severe ecological implications. A variety of carbon capture and storage (CCS) technologies are under development to help achieve these decarbonisation goals although only a limited number of projects exist globally. In the UK, the Energy Act 2008 sets out offshore gas storage laws, and licensing is regulated by the North Sea Transition Authority. At present, storage can only take place offshore in saline formations or depleted oil and gas fields and no commercial projects exist (Harper, 2011). A range of carbon

utilisation approaches have been developed, presenting an opportunity to valorise carbon and accelerate CCS growth.

1.3 Geothermal energy

Geothermal energy is heat from within the Earth that is sourced both from the radioactive decay of elements such as uranium and thorium, and residual heat from the accretion of the Earth. The heat can either be used directly, such as for district heating systems, or it can be used indirectly, to produce power. Geothermal energy is widely untapped and accounts for only a small portion of global power production by renewables. Installed capacity reached 13,900 MW in 2019 which is equivalent to just 0.5% of the renewable energy mix (IRENA 2020). Current growth rates of geothermal power production remain low in comparison with other renewable energy sources - at about 2% in 2020, which was below the average growth of the five previous years (IEA 2021a). Advantages of geothermal energy such as a high capacity-factor and the ability to supply baseload energy compete with long project completion lead times, high site specificity (traditional extraction technologies are restricted to locations with high geothermal gradients), and high upfront costs as factors influencing this lacking growth to date.

Of the power produced by geothermal energy, the majority derives from conventional hydrothermal settings. Dry steam, flash steam and binary cycle power plants are mostly located at hotspots or along tectonic plate boundaries where there is a high geothermal gradient, meaning temperatures are higher closer to the surface than on average. As cost increases with drilling depth, these geothermal resources are preferable to deeper resources at the same temperature, found away from conventional hydrothermal locations. In an indirect-use hydrothermal plant, for example, heated water is converted to steam which turns a generator's turbine to produce electricity.

The concept of 'hot dry rock' or 'enhanced geothermal systems' (EGS) has been developed to target hot formations that are not necessarily aquifers (Mortensen, 1978). EGS involves hydraulic fracturing to form an artificial reservoir with enhanced permeability, enabling the flow of an injected working fluid into the formation, where it heats and surfaces via a

production well. CO_2 has been proposed as a working fluid for EGS (Brown, 2000). CO_2 becomes a supercritical fluid after surpassing the temperature and pressure thresholds of 31 ºC and 7.4 MPa respectively, where it has both gas-like and liquid-like properties. In this state, CO_2 has a lower kinematic viscosity than water, resulting in increased fluid flow rates and consequently improved heat extraction rates. Since CO_2-EGS enables heat to be mined from hot fractured rock by using CO_2 as a working fluid, a wider range of geothermal heat sources can be targeted for electricity production. This includes impermeable crystalline basement rock and low-medium grade geothermal resources which cannot be effectively exploited using conventional geothermal techniques. Further, CO_2-EGS may be combined with carbon storage (Pruess, 2006); CO_2 can be ultimately stored in a reservoir that has become thermally depleted due to the continuous injection of cooled CO_2 back into the reservoir over time, making the geothermal energy extraction process no longer economically feasible.

1.4 CO_2-plume geothermal

CO_2-plume geothermal (CPG) is a more recent approach combining CO_2 storage with geothermal heat extraction (Randolph and Saar, 2011) and is perhaps the most viable option for the utilization and storage of industrial quantities of CO_2. Most uses of CO_2 consume energy in the process, and the 40 Mt stored annually by 26 commercial CCS facilities around the world (Global CCS Institute, 2020) is just 0.013% of estimated energy-related CO_2 emissions in 2020 (IEA, 2021b). Enhanced oil and gas recovery (EOR and EGR) are established methods that can facilitate the storage of large amounts of CO_2. However, there is a tradeoff between CO_2 storage and emissions as a byproduct of additional oil and gas production. By contrast, CPG proposes the use of CO_2 to produce near zero carbon energy followed by the storage of large quantities in the subsurface. Distinguished from CO_2-EGS, CPG does not rely on fracking to enhance permeability at the risk of induced seismicity. Instead, high-permeability and high-porosity formations with low-permeability cap rocks, within sedimentary basins, are targeted (Figure 1). Examples of such formations include saline aquifers and hydrocarbon reservoirs, which have higher pore-volumes than artificial EGS reservoirs – a key factor for CO_2 storage and geothermal potential. Cooled CO_2 fluid is injected into the subsurface via an injection well where it displaces in situ fluid and becomes

heated. A portion of the fluid is returned to the surface via a production well at an increased pressure and temperature which can be used to generate power in a surface plant. In a direct CPG system, CO_2 is expanded through a turbine whereas in an indirect system, CO_2 is sent through an exchanger to heat a secondary working fluid – both systems can be used to produce power.

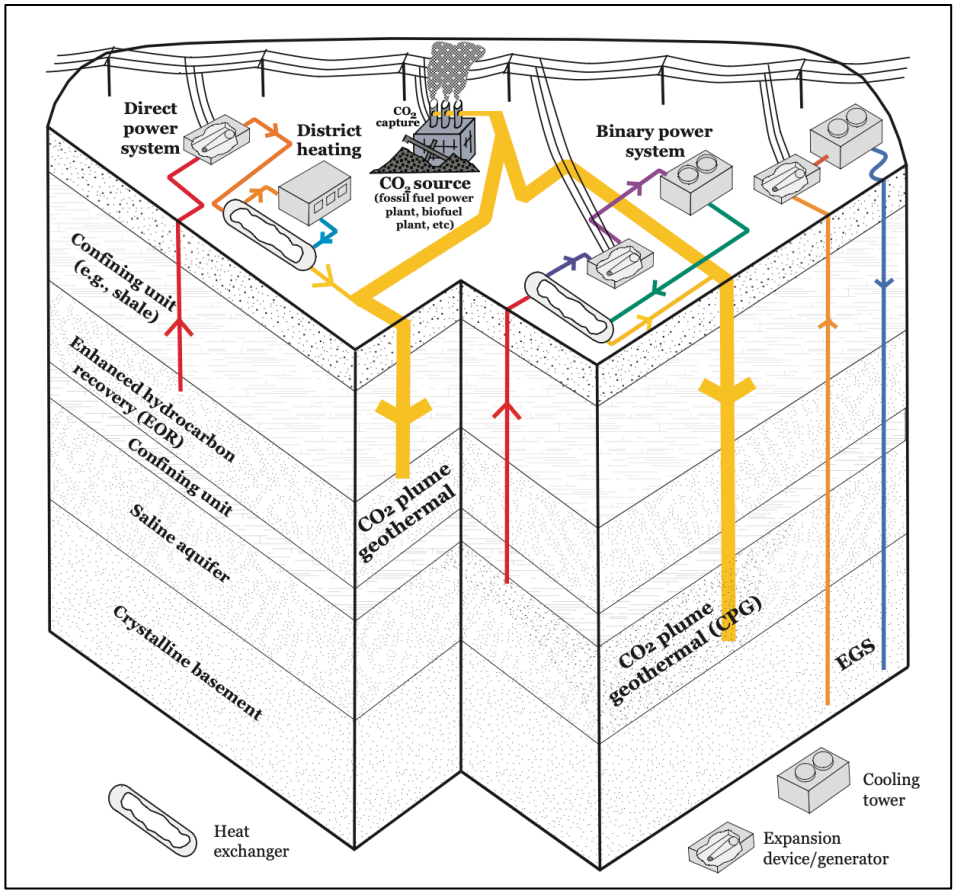

Fig. 1: Illustration of potential CO_2-based geothermal systems (Randolph and Saar, 2011)

The thermosiphon effect is distinctive feature of CO_2-based geothermal energy extraction systems like CPG, although it is not necessary for power production. CO_2 density is sensitive to small changes in pressure and temperature as CPG systems operate near the critical point (7.38 MPa and 31 °C). Since cooled CO_2 is injected and CO_2 heated by the reservoir is produced, a high-density difference between the wells occurs. Consequently, a buoyancy driven thermosiphon (plume) forms, self-circulating fluid around the system and eliminating additional parasitic pumping requirements for power generation. On the other hand, water-based systems have a lower thermal expansivity coefficient and only form weak thermosiphons in deep and hot reservoirs.

Different areas of CPG have been studied in the literature. This includes wellbore processes, effects of varying reservoir conditions, fluid and thermal dynamics, fluid-rock chemical reactions, economic analyses, and comparisons with conventional geothermal power systems.

The CPG concept was first proposed in (Randolph and Saar, 2011). In this paper, CPG systems are tested against conventional water-based systems and EGS. Fluid-mechanical simulations suggest that CPG has higher heat energy extraction performance under a broad range of conditions, supporting the idea that the potential of geothermal energy is not fully realised. A wide range of resources can be targeted for the CPG power cycle, including those that can be classified as 'low-moderate' geothermal resources (Lee, 1996) as CPG can use temperatures below 150°C at greater depths than classical hydro-geothermal (Adams, 2015). Additionally, CPG was initially considered as a way to offset the costs of geologic carbon sequestration by calculating electricity generated per ton of CO_2 sequestered (Randolph and Saar, 2011b). CPG was found to provide larger CO_2 storage capabilities and more efficient electricity production than CO_2-EGS. The reservoir simulator TOUGH2 with equation-of-state module ECO2N has been widely used (Pruess, 2004) in initial CPG performance studies to simulate either a five spot well configuration or well-doublets. Reservoir-carbon storage scenarios with and without prior geothermal heat extraction using CPG are compared in (Randolph *et al*., 2013) to observe the effects of thermal drawdown. Results suggest that about 10% of reservoir over-pressurization caused by subsurface fluid storage can be removed in the CPG scenario. Mechanical stresses and deformation can occur in the reservoir and cap rock due to increased pressure after CO_2 injection, which can change how the reservoir stores CO_2, as well as how CO_2 flows in the reservoir. With increasing pressures, the risk of fault slip can escalate, which in turn can lead to CO_2 leakage (Goudarzi, 2016).

In subsequent studies further examining CPG processes, wellbore heat transfer has been considered to validate an assumption made in the analyses of the aforementioned studies - that wellbore heat transfer can be assumed to be adiabatic. Wellbore heat loss was found to move down to >5% within a few days of operation (Randolph *et al*., 2012). By coupling wellbore processes with reservoir processes when modelling CO_2-based geothermal energy extraction, (Pan *et al*., 2014) evokes a discussion on optimizing injection and production flow rates for power production and setting up a thermosiphon. The model considers heat transfer in the well and the surrounding formation, as well as frictional, inertial, and gravitational

forces. It was concluded that with higher injectivity flow rates, there is a decrease in lateral heat gain from the surrounding rock to the wellbore, leading to colder and denser CO_2 being injected into the reservoir. As a result, a smaller wellhead pressure is required to maintain the well-bottom pressure, driving flow into the reservoir ultimately making establishing a thermosiphon easier when injection rates are higher. Likewise, a higher production well flow rate results in a higher production wellhead temperature. However, if this flow rate becomes too high, reservoir pressure losses due to extensive cooling as well as pressure losses due to increased friction between working fluid and the well wall would preside, thereby eliminating the advantage of decreased lateral heat exchange that comes with a higher flow rate. This tradeoff should be considered when selecting the mass flow rate of a CPG system for optimised power production.

In addition to wellbore heat transfer and flow rates, well spacings can be configured to provide the largest average electricity generation over time for a CPG system. When wells are too close together, peak electricity generation increases while the reservoir cools down faster. On the other hand, when wells are spaced too far apart, heat is maintained in the reservoir for longer whereas there is more resistance to flow through the reservoir, meaning peak electricity generation decreases. (Adams *et al*., 2021) uses fluid pressure drop and temperature decay characterizations of sedimentary radial reservoirs to calculate CPG power generation under a range of parameters including well pipe diameters and reservoir radii (well spacings). For a 300 m thick reservoir, a reservoir radius of 707 m provides enough heat maintain power generation over 50 years.

Thermosiphon strength in a CPG system is much greater than a system that uses brine as a working fluid, so much so that a CO_2 thermosiphon converts approximately 10% of the energy extracted from the reservoir to circulating fluid. As a result, pumping power requirements can be eliminated altogether across a range of geothermal gradients and reservoir permeabilities (Adams *et al*., 2014). In this 2014 study, indirect geothermal systems are exclusively modelled where the heated working fluid drives a secondary Rankine cycle. By contrast, direct systems expand the working fluid through turbomachinery to generate electricity and are preferable when a high pressure-difference between injection and production wellheads is observed – as in a CPG system. Direct CO_2 systems have been shown to have a higher power output than both indirect CO_2 and direct brine-based geothermal systems at a range of depths and permeabilities (Adams *et al*., 2015). The

significant impact of well diameter on the mass flow rate and the power output of a CPG system is also indicated in this literature. Typical oil and gas well diameters (0.14 m) produced small amounts of power, however increasing the well diameter from 0.27 m to 0.41 m resulted in a 90% increase in power, demonstrating the power output sensitivity to well diameter in CPG systems.

Prior to research undertaken by (Garapati *et al*., 2014), studies had not considered in detail how the multi-layered nature of sedimentary reservoirs might impact CPG performance. In this study a numerical reservoir model is devised to determine the effect of the position of horizontal geologic layers, each layer varying in horizontal permeability, on heat extraction performance. When the permeability of the bottom layers of the reservoir decreases, heat extraction rates are found to decrease. As the permeability of the bottom layers increases no change is observed. Additional aspects of the CPG system were found to be affected by reservoir permeability heterogeneity. For example, where a lower permeability layer is found on top of a higher permeability layer, the pore fluid pressure drop between injection and production wells increases leading to lower CO_2 mobility and, in turn, a weaker thermosiphon. Further, the mass fraction of CO_2 produced at the production wellhead also depends on the stratigraphic position of highly permeable layers. In a more recent analysis of fluid and thermal dynamics in heterogenous reservoirs to assess CO_2-based geothermal energy extraction, geological and geothermal conditions specific to the Songliao Basin, China, are considered (Xu *et al*., 2017). By modelling reservoir porosity and permeability heterogeneity, it was determined that CO_2 migration pathway and fluid flow processes can be significantly affected depending on the location of highly permeable zones. When a highly permeable zone exists between two wells, injected CO_2 is likely to flow through this zone to reach the production well. The nature of this flow pattern is attributed to the high mobility of CO_2.

Fluid-rock geochemical reactions have the potential to affect the performance of geothermal systems. Mineral dissolution, precipitation, and associated changes in porosity can impact factors such as fluid flow, heat transfer, and reservoir longevity. In a CO_2-based system, three fluid phases can be distinguished in the reservoir. First, an inner zone in which no aqueous phases exist, having been removed by dissolution into the flowing stream of supercritical CO_2. Second, an intermediate zone, consisting of a two-phase CO_2 water mixture, surrounding the inner zone. Third, a peripheral zone made up of a fluid of a single aqueous

phase with dissolved CO_2 (Ueda *et al*., 2005) (Xu *et al*., 2014). Accordingly, varying geochemical reactions occur between CO_2 and rocks both with (zones two and three) and without (zone 1) the presence of water. In one study (Xu *et al*., 2014), reactive geochemical transport models were designed to assess CO_2-induced mineral alteration and its influence on circulation in a CPG-type system. Results found that the dissolution of chlorite bearing Mg- and Fe- can lead to the precipitation of carbonate minerals in the context of a sedimentary basin, trapping some CO_2 in turn leading to a decrease in porosity over the first 10 years of geothermal energy extraction. Although no significant reservoir damage was observed for the cases in this study, the effects of primary mineral composition on heat extraction performance in any given reservoir should still be considered. Salt precipitation particularly exacerbates the effects of these CO_2-water-rock geochemical reactions on heat mining rate; continuous CO_2 injection can cause water to evaporate into the CO_2 phase which can result in a high water-saturation gradient near the injection well and a high gas-liquid capillary, leading to the back flow of formation water into the injection well. This backflow may lead to dissolution of anthorite into the formation water near the injection well, for example, as backflow can prevent water from dispersing from this area consequently prolonging geochemical reaction times and inducing further mineral changes (Cui *et al*., 2017).

Besides influencing certain geochemical reactions, increased salt precipitation accumulation around the injection well due to backflow is a risk to heat extraction performance in CO_2-based geothermal systems by decreasing porosity and permeability (formation plugging) (Borgia *et al*., 2012). Remedies for this problem have been proposed, including injecting low salinity water prior to CO_2 and injecting water vapor during CO_2 injection. Site-specific conditions can also be optimised: a reservoir with high temperature, high porosity and permeability, and an appropriately high injection-production pressure difference is optimal for reducing the negative effects of salt precipitation (Cui *et al*., 2017). Additionally, salt precipitation effects have been tested for different geothermal settings; for example - depleted natural gas reservoirs (Cui *et al*., 2016), finding that the same mitigation strategies can apply.

Brine displacement by injected CO_2 is another component of CO_2-based geothermal systems that has been studied for its potential effects on heat energy extraction rate (Garapati *et al*., 2015). In this study, the CPG concept is defined by two main operational phases. First is the process of establishing a plume by injection of CO_2 by displacing the existing brine. Second is the circulation of the working fluid together with the reinjection of cooled CO_2, closing the

power loop. In the first stage, water can dissolve into the CO_2 and CO_2 can dissolve into water. Dissolution at this brine-CO_2 interface is shown to have minimal effects on fluid circulation and overall CPG performance. Overall, brine displacement simulations demonstrate that long-term geothermal energy extraction can take place using only a finite amount of CO_2, although the amount of CO_2 to do so increases with reservoir depth, permeability, and well spacing. Before the working fluid is reinjected into the reservoir, brine can be separated and injected away from the plume to better control and direct the plume pressure field and flow direction. In a study combining geothermal energy extraction with CO_2 storage to manage reservoir over-pressurization due fluid injection (Buscheck *et al*., 2013), it is suggested that removing residual brine before reinjection helps prevent reservoir deformation, fracturing, CO_2 leakage, and reduced injectivity, since brine cannot accumulate around the injection well as it has a lower mobility than CO_2.

In early research, surface plant power generation models for estimating CPG system performance generally work under the assumption that the fluid produced from the reservoir is pure, dry CO_2. However, particularly in the case of deep saline aquifers as a setting for CPG, some fluid entering the production well contains dissolved H_2O, originating at the interface of the plume, or the peripheral zone. (Fleming *et al*., 2020) investigates the ways in which this 'wet' CO_2 behaves in a production well of a CPG system, and its effects on power production. H_2O is shown to exothermically exsolve in the production well since the solubility of H_2O in CO_2 is reduced with decreasing temperature and pressure. This process increases the temperature of the CO_2 fluid while liquid water is coproduced at the wellhead. A higher fluid temperature corresponds to higher turbine power output, increasing the overall system efficiency. Therefore, calculations omitting exothermic water exsolution may underestimate actual power output of a CPG system in the presence of water.

1.5 CPG in natural gas reservoirs

Natural gas reservoirs are a potential target for CPG energy extraction (Randolph and Saar, 2011). Like deep saline aquifers, natural gas reservoirs are porous and permeable by nature, and are sealed by a low permeability layer. These natural reservoirs occur in sedimentary basins and are large in volume, making them an appropriate choice for carbon storage in

addition to geothermal energy extraction. CPG in natural gas reservoirs can be further integrated with enhanced gas recovery operations, bridging the gap between conventional natural gas recovery (CNGR) and CPG, offering economic advantages.

More recent literature suggests that depleted, high temperature gas reservoirs are also advantageous over deep saline aquifers for geothermal exploitation as pore-water content is usually much lower, meaning risk of reservoir damage by salt precipitation is lowered (Cui *et al*., 2016). By extension, the absence of pore-water helps to mitigate the water production process that occurs during the CPG setup process in saline aquifers (Zhang *et al*., 2017). In both studies CPG is coupled with CO_2-enhanced gas recovery (CO_2-EGR) which takes place before geothermal energy extraction begins, ensuring the gas reservoir has a minimal methane content so that CPG performance does not become compromised if excess methane is present in the working fluid. Additional advantages of combining these carbon utilisation and storage technologies include reservoir re-pressurization after CNGR which is necessary for CPG, and economic benefits that come with the production of additional methane. Crucially, natural gas is an important fossil fuel for continued production in the energy transition period when compared with oil and coal, as it produces lower carbon emissions when combusted.

Carbon storage has been coupled with enhanced gas recovery as a way to reduce net costs relative to CO_2 storage alone (Patel *et al*., 2016). The CO_2-EGR concept would proceed after natural gas production rates have become too low and are no longer economically feasible using CNGR methods. This scenario is caused by the pressure reduction that occurs as CNGR takes places, however, significant amounts of gas may remain in the reservoir. CO_2-EGR involves sweeping methane to production wells by the injection of CO_2, which can displace the methane, partly because CO_2 has a density which is about six times that of CH_4 (Goudarzi, 2016). Notably, at typical moderate-depth reservoir conditions, the fluid-phase CO_2-CH_4 mixture is supercritical with gas-phase diffusivities, so significant mixing can occur during CO_2-EGR. In this case, the value of natural gas in the reservoir decreases and breakthrough of CO_2 at the production well is accelerated. Some injection and production strategies have been developed to decrease mixing (Patel *et al.,* 2016).

One study reviewing issues around the injection and storage of CO_2 in depleted gas reservoirs was based on characteristics of a typical Southern North Sea setting. In particular, the

pressure response of gas reservoirs during depletion was analysed. It concluded that the level of aquifer response that occurs in a reservoir can influence the gas recovery factor and abandonment pressure. When a gas field is produced and there is no aquifer response (no water drive), recovery is upwards of 90% and abandonment pressures are low, creating more optimal conditions for CCS as CO_2 can be injected into this pressure 'sink' (Hughes, 2009).

A non-isothermal effect resulting from CO_2 injection activity in depleted gas reservoirs is Joule-Thompson cooling, which occurs when high pressure gradients exist around the injection well. When moving from a high pressure to a low pressure at constant enthalpy (thermally insulated with no heat flow across system boundaries) the working fluid experiences a temperature drop (Han *et al*., 2010). This effect is especially important to consider in depleted gas reservoirs as pressure decreases as production continues and fields are abandoned when conventional gas recovery methods are no longer viable. Using an analytical solution to determine the risk of JT cooling for an injection rate of 3 kg/s (95,000 t/annum) and moderately warm temperatures (>40 ^{o}C) (Mathias *et al*., 2010) concluded the effect to be likely negligible for initial reservoirs pressures >2 MPa.

In contrast to prior reservoir modelling that has investigated the effects of decreased pore-water content in natural gas reservoirs on salt precipitation, (Ezekiel *et al*., 2020) further develops ideas from reports on CPG combined with enhanced gas recovery in natural gas fields. Thermodynamic wellbore processes, heat extraction rates, and surface plant power conversion are considered for a proposed carbon capture double-utilization and storage system (CCUUS). Aiming to valorise CO_2 two-fold, these technologies could be combined to extend the useful life of ageing natural gas fields and, in turn, offset the costs of CCS. Important synergies of this system include a shared working fluid and drilling infrastructure. (Ezekiel *et al*., 2020) assesses the feasibility of their proposed CO_2-EGR-CPG system by using a numerical model of an anticlinal, non-compartmentalized natural gas reservoir at 150 ^{o}C. A timeframe for electricity generated at each stage is developed with a peak of 2 MWe observed during the longest (35 years) CPG stage. Results also show that direct CPG systems have a higher electric output than indirect systems (organic Rankine cycles).

(Cui, *et al*., 2020) gauges the suitability of natural gas reservoir conditions for CO_2-based geothermal energy exploitation compared with water-based exploitation, as well as highlighting some site-specific problems that could be encountered for natural gas reservoirs.

Results for natural gas reservoirs at 140 ºC are congruent with those concluded by studies of CPG performance in deep saline aquifers; CO_2 has a better performance than water at most reservoir conditions and operating conditions, even when water saturation levels are high. However, for high permeability gas reservoirs with high salinity and high water-saturation (serious risk of salt precipitation), the superiority of CO_2 as a heat transmission fluid over water is not as clear-cut. (Cui *et al*., 2021) undertakes a whole process analysis from operation processes to economic analyses for the geothermal exploitation of depleted high-temperature gas fields at 120 ºC. Composition of produced gas, pressure and temperature are analysed for the CO_2-EGR-CPG process. A heat mining rate of about 10 MWth can be maintained over 30 years when the injection-production difference is 6 MPa. A CO_2 direct cycle system is found to be most optimal for heat extraction.

1.6 Summary

Increasing the portion of renewables in the energy mix is key to reducing carbon emissions. Geothermal energy is a very low-carbon energy source that renews much faster than the geological times required fossil fuels formation with the ability to supply baseload power due to the constancy of subsurface temperatures. That said, geothermal is widely untapped since high temperature resources are not commonly available at relatively shallow depths. Research into CO_2-based geothermal energy extraction has led to the proposal of CPG, a concept which is designed to extract heat from porous and permeable sedimentary basins using CO_2 as an alternative working fluid to brine, ultimately storing industrial quantities of captured carbon. Supercritical CO_2 (sCO_2) has a high thermal expansivity which causes large density differences between the injection and production wells of a CPG system, generating a thermosiphon that can circulate sCO_2 around the reservoir. The low kinematic viscosity of sCO_2 brings about higher mass flow rates. These properties equate to the increased heat extraction performance across a range of reservoir and operating conditions when compared with hydrothermal systems. Consequently, untapped geothermal reservoirs characterised by common geothermal gradients could be accessed by implementing CPG so resources that were previously considered to be unrecoverable can be targeted for efficient and economical energy extraction. Natural gas reservoirs have been proposed as geothermal resources which could be exploited by CPG systems, although, few geographical case studies exist (Gupta and

Vashistha, 2016) (McDonnell *et al*., 2020). Natural gas reservoirs are particularly suited to CPG systems since impermeable cap rocks are proven seals for the safe storage of high volumes of CO_2 and CPG can be neatly integrated with EGR.

2. The study area: Southern North Sea, UK Continental Shelf

2.1 Geology

The Southern North Sea Basin is the main gas producing area on the UK continental shelf. Carboniferous, Permian, and Triassic age sandstone reservoir fields have all been successfully developed in the Southern North Sea with gas sourced from Upper Carboniferous coals (Cornford, 1990). Northerly continental drift during the Carboniferous Period brought Laurussia into the equatorial belt, where swamps and delta tops abounded. For the Southern North Sea (SNS) area, this was a period of back-arc rifting resulting in rapid subsidence and accommodation space, leading to the deposition of the Upper Carboniferous Coal Measures Group which is the primary source of gas in SNS fields. Some gas is also derived from deeper intervals within the Lower Carboniferous (Monaghan et al., 2017). The end of the Carboniferous was marked by the Hercynian Orogeny, a continental collision between Laurussia and Gondwana that closed the Rheic Ocean to form Pangea. A major foreland basin formed ahead of the rising mountain front, stretching to the SNS and beyond (Underhill, 2003). Continued compression, shortening, uplift, and erosion across the Hercynian foreland is conducive to the substantial burial depths achieved at this time, particularly for Lower Carboniferous rocks.

By the beginning of the Permian (also a period of rifting), the UK was in the middle of Pangea, and a large part of contemporary Europe was below sea level within E-W trending inland basins, one of which is the Southern Permian Basin (SPB). The SPB stretches from Cheshire to Poland, about 1500 km (Glennie, 1998). Located in the arid northern hemisphere desert belt (Glennie, 2007), there was little sediment in this basin, and high erosion rates resulted in a degree of peneplanation. Aeolian sands deposited around residual hills in the basin made up the initial basin topography. Subsequently, the basin periphery was infilled with aeolian and ephemeral-fluvial sands, known as the Rotliegend Leman Sandstone Formation. This unit is the main productive reservoir of gas fields in the southern half of the SNS (Figure 2). The centre of the basin was occupied by playa lakes with evaporites which formed after periods of wetting and drying. The Silverpit Formation lies north of the Leman Sandstone Formation in the same basin. While this clay-dominated formation has no reservoir potential, it seals gas stored in the underlying Carboniferous reservoir sandstones

(Gast et al., 2010). Early discoveries were produced from the Rotliegend sandstone reservoir and subsequent wells were drilled further north – discovering gas-filled Carboniferous sandstones. The Rotliegend reservoir usually lies above and on top of Carboniferous sandstones, mudstones, and coals. Where it lies directly upon sandstones, there is commonly a continuous gas column existing between the two. As these underlying Carboniferous reservoirs are generally much lower in permeability, they have not been typically produced, leading to the clear spatial distinction seen on the map (Figure 2). The Cygnus Field (Dredge and Marsden, 2020) is an exception to this trend since there is older basal sandstone reservoir in the Permian, which is found further north.

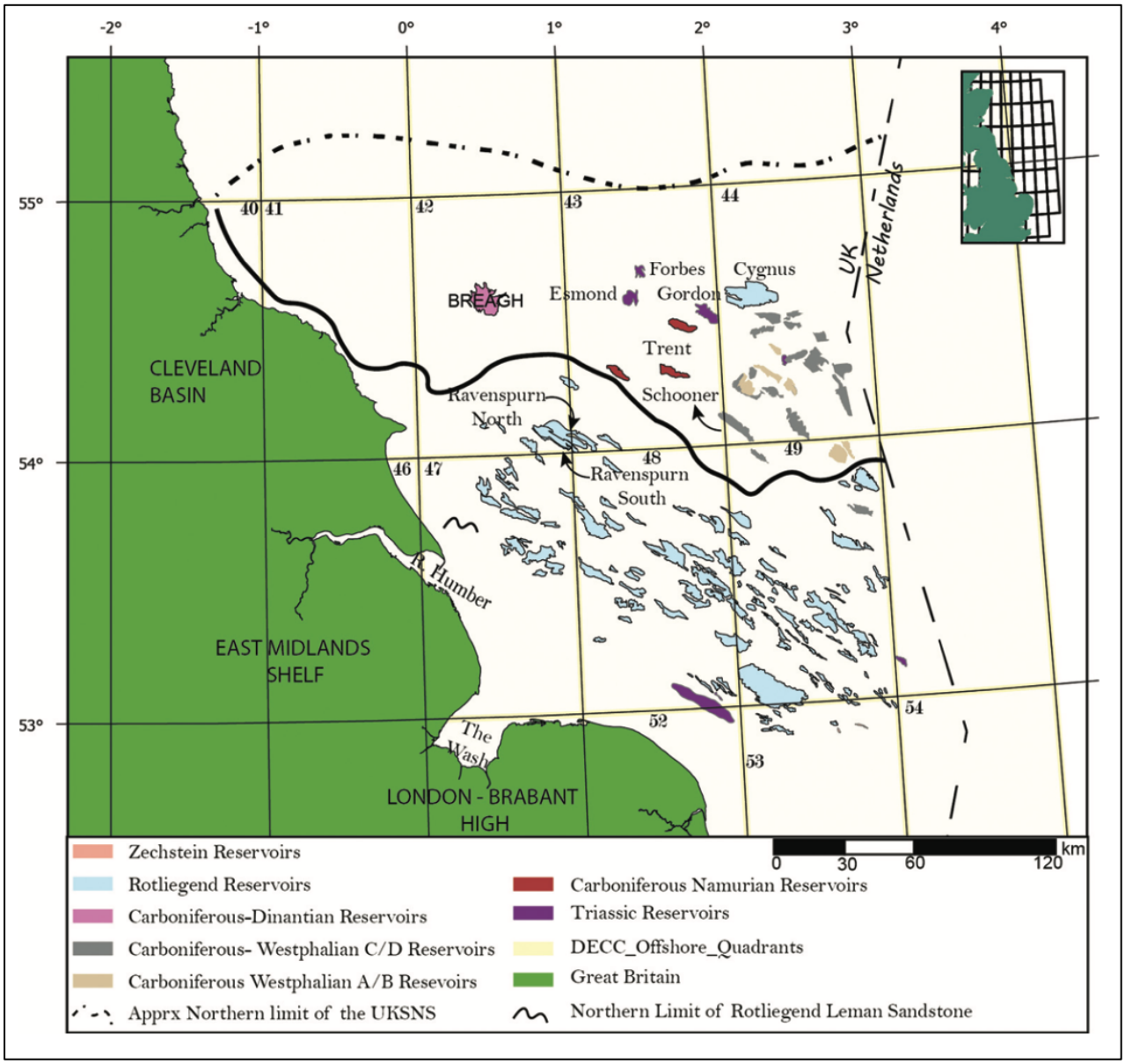

Fig. 2: Overview of gas fields in the Southern North Sea (Nwachukwu et al., 2020)

Continuing to the Late Permian, a connection was established with the Tethys Ocean, marine water from which filled the whole basin. With little run off from the adjacent land, carbonate precipitation followed, accounting for the dolomite in the area. However, the connection was not continuous, and so the basin dried out periodically. As a result, there are at least five deposition cycles of evaporite salts (carbonite, anhydrite, halite, sylvite) and sediments (stinkstien, black shale, carbonate-rich shale). Together, these cycles make up the Zechstein Group and effectively seal the Rotliegend Leman Sandstone reservoir of SNS gas fields.

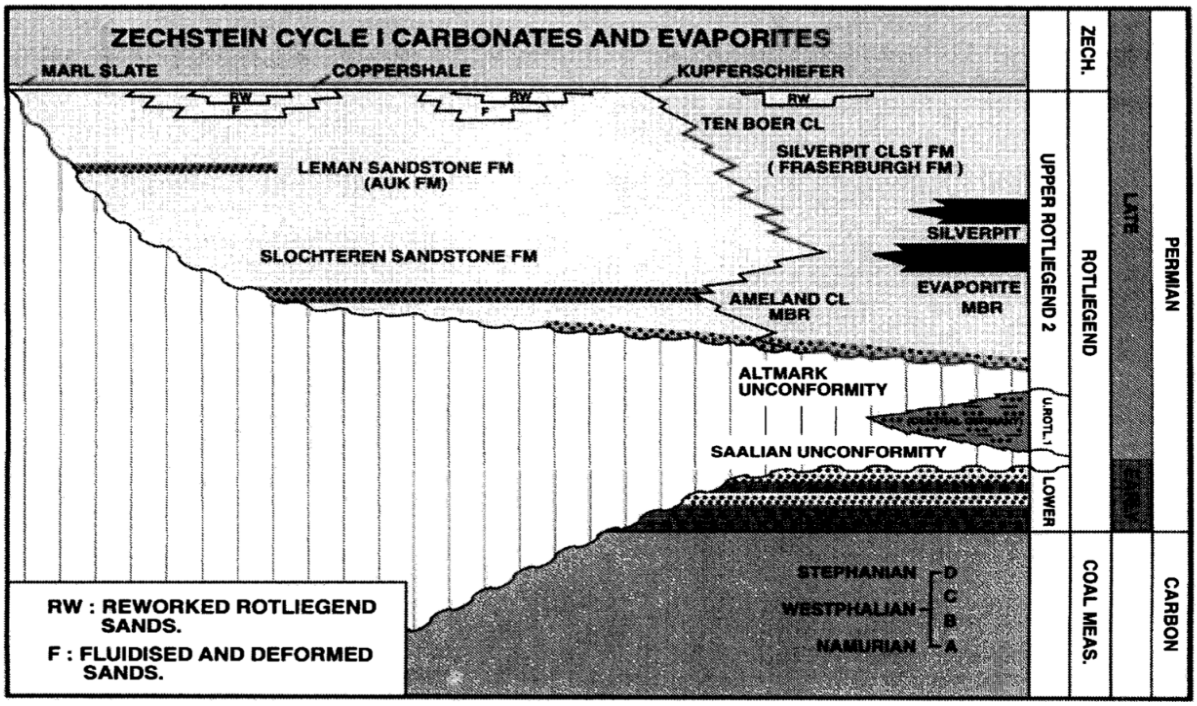

Fig. 3: Stratigraphic diagram of Permian and Carboniferous groups of the North Sea Area (Glennie, 1998)

The third major productive interval in the SNS derives from the Triassic Period. Rifting and burial also took place throughout this time, with rifting associated with the beginnings of the Atlantic Rift. The whole succession broadly constitutes of a lower sandstone group and an upper mudstone group. The Bunter Sandstone Formation, a member of the sandstone group, was deposited in an extensive north-south fluvial system and was later overtopped by ephemeral lake deposits, similarly to the Permian (Gluyas and Bagudu, 2020). This formation makes up a reservoir interval in some fields such as Hewett (Hook, 2020). Gas charge occurs in areas of salt withdrawal, where the Triassic reservoir sandstone touches down on the Permian strata, allowing migration to occur. Following on to the Jurassic, strata is scarce in

the SNS (having been eroded or not deposited), although Late Jurassic extensional basin development proceeded by post-rift thermal subsidence allowed the Carboniferous Coal Measures to be buried deep enough to mature (Underhill, 2003). Chalk is also variably present, with Jurassic through to Tertiary units present at the seabed.

2.2 Gas production

About 90% of UK continental shelf (UKCS) dry gas reserves are found in the SNS area, with current reserves from SNS fields estimated to be 2696 bcf (OGA, 2019). Gas production from the UKCS met almost two thirds of the total domestic energy demand in 2019. However, overall production is in decline and the UK now relies heavily on imports, with LNG making up 39% of all imports in 2019, up from 15% in 2018 (BEIS, 2019). Factors like high rig decommissioning costs and a national objective to achieve maximum economic recovery of UKCS resources (MER UK) (Wood, 2014) emphasise the importance of research into extending the useful lifetime of SNS gas fields, as LNG imports clearly have negative implications for decarbonisation goals.

Gas fields in the SNS have a high estimated theoretical potential, which can be defined as 'heat in place' (Rybach, 2015). A portion of this heat could be extracted for electricity generation using CPG. Platforms situated on the UKCS make appropriate infrastructure for CPG systems since they can benefit from high bottom hole temperatures as the Earth's crust is thinner than it is onshore, meaning on average, geothermal gradients are higher. The average UK geothermal gradient onshore is 26 °C km^{-1} (Busby, 2013). From data gathered on a range of gas fields in the SNS for this study, an average geothermal gradient of 30 °C km^{-1} was observed. Importantly, a full spectrum of data collated over years of industry experience in the SNS has been published, which is essential for characterising and assessing the electricity generation potential of a CPG system. Often included in this data are peak flow rates associated with gas production, for example, indicating that reservoir permeability architecture may be suitable upon initial inspection.

In the immediate vicinity of producing SNS gas fields, a significant number of windfarms are being planned, constructed, and operated. A growing presence of electrical infrastructure

including substation platforms and subsea cables has created an opportunity for ‘gas to wire’ technology (OGA, 2018) to exploit the ullage in power that windfarms experience with variations in weather. Particularly for isolated and abandoned fields that are no longer connected by pipelines, electricity produced by CO_2-based geothermal energy extraction could also take advantage of these windfarm networks. The potential opportunity of dispatching electricity generated by CPG via existing and planned electrical infrastructure in the SNS could be capitalised on to supply power onshore, or to meet the power requirements of producing gas fields in the area.

3. Methods and data

3.1 Resource classification and reporting

The United Nations Framework Classification for Fossil Energy and Mineral Reserves and Resources (UNFC) (ECE, 2013) is a universally acceptable scheme for classifying and reporting fossil energy and mineral reserves and resources. In 2016, specifications for the application of UNFC to geothermal resources were published (Falcone *et al*., 2016) in accordance with UNFC renewables specifications (Denelle *et al*., 2016). These documents are used in conjunction to classify the target geothermal resource of this study, and, in doing so, support the normalisation of consistent reporting of geothermal resources. Consequently, the findings of this study may be included in wider-scale resource management and energy studies, for example, in which the resources of an area or nation must be aggregated.

UNFC geothermal specifications (section C.12) presents the resource classification process as:

1) Defining a project associated with a geothermal energy source
2) Estimating quantities of energy that can be recovered and delivered as a geothermal energy product by the project
3) Classifying the geothermal energy resource based on the criteria defined by the 'E, F and G' categories

CPG is a system designed to produce electrical energy, contrary to direct-use geothermal systems. Thus, the geothermal energy product in this instance is power, reported in kilowatts electric (kWe). The geothermal energy source and the associated project are defined in Section 3.2 to facilitate the choice of a suitable energy quantification method (Falcone and Conti, 2019). The energy quantification method and inspection of all accompanying data is set out in Sections 3.3 and 3.4, respectively. The geothermal energy product is then quantified in Sections 4 and 5. Finally, the UNFC criteria are used to classify the quantities using a simple coding scheme. These are economic and social viability (E), field project status and feasibility (F), and geological knowledge (G). The resulting class reflects the associated level of confidence in the potential recoverability of the quantities.

3.2 Defining the geothermal energy source and the project

The project is a development or operation, in this case conceptual, that transforms the geothermal energy source into a useable geothermal energy product, laying the foundation for economic appraisal and decision making. It is defined so that a suitable energy quantification method can be established.

In this thesis, the project, along with the geothermal energy source, is referred to as the 'CPG system', which consists of 3 main elements: the reservoir, wells, and surface plant (Figure 4). The thermal energy contained in a depleted natural gas reservoir, now assumed to be fully saturated with CO_2, is the geothermal energy source. In practice, the mass fraction of the contained fluid is mostly CO_2 (upwards of 96 %), water or brine, and CH_4 (Ezekiel *et al*., 2020). The reservoir rock density, heat capacity, thermal conductivity, permeability, and porosity are also assumed to be homogenous. The effects of faults and fracture networks on CPG performance are outside the scope of this study. In a real system, thermal depletion would naturally occur as heat is mined over time, and heterogenous layers exist throughout the reservoir rock which can affect CPG performance. Simplifying the geothermal energy source in this way means power production can quantified using straightforward calculations.

Wells and a surface plant make up the project which is theoretically structured around an existing offshore drilling platform. An injection-production well doublet is chosen as the base-case well configuration because it is easily scalable. Wells are drilled out at an angle from a single location at the surface (mean sea level) to reach reservoir depth, 707 m apart, so piping at the surface is minimised and the injected fluid can sufficiently heat to the reservoir temperature. 707 m is chosen since this distance has been demonstrated to sustain power over a period of 50 years at a reservoir temperature, pressure, thickness, and permeability similar to that of SNS gas fields (Adams *et al*., 2015), and few other distances have been trialled. An inner well diameter of 0.14 m is selected for the base-case since it is typical of oil and gas wells (Ezekiel *et al*., 2020). The direct CPG surface plant employed in this study consists of a sCO_2 turbine and a shell and tube heat exchanger, and no surface pump is used in the base case. The effect of pumping on power generation is discussed in Section 5.2 and the effect of varying well diameter on power generation is determined in Section 5.3.

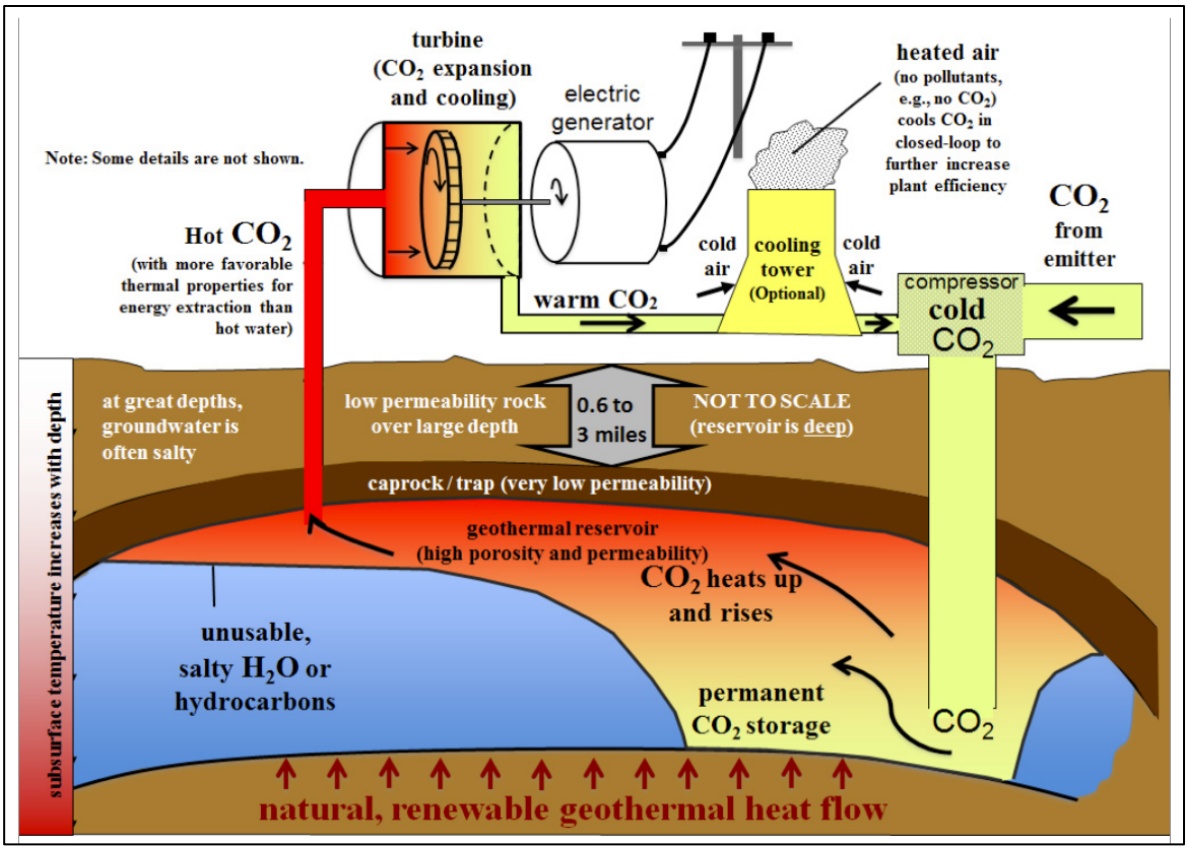

Fig. 4: Direct CPG system illustration (Garapati et al., 2014)

3.3 Quantifying CPG power production

Each UKCS gas field in the SNS represents a potential geothermal energy source from which quantities of energy can be extracted by the defined project. The reservoirs of individual fields can be characterised across a range of parameters which are set out in Section 3.4. Since the values of these parameters vary from field to field, some are better suited for CPG than others. In this thesis, a 'first order' screening analysis is carried out (Section 4) to select a target field for the main analysis (Section 5), where power generation for the selected field is estimated with increased accuracy. The target field is chosen as the most suitable geothermal energy source from which quantities may be recovered by the project in terms of power generation potential and practicality. In the screening analysis, power generation is deduced from each field's reservoir temperature and pressure values alone. In the main analysis, the thermosiphon effect, as well as the frictional pressure losses that occur as CO_2 moves through the CPG system, are also considered.

3.4 Data

A desk study is carried out to collate data on UKCS SNS gas fields. In this non-experimental quantitative research, the independent variables are equivalent to a set of conditions that characterise the geothermal energy source and govern CPG performance. The dependent variable is ultimately the geothermal energy product quantity that can be recovered by the project. Generally, independent variables are not manipulated and the dependent variable is simply evaluated. In other words, this research does not focus on tracing cause and effect relationships between variables. An exception to this is the varying of well diameter (an independent variable related to the project) on power production. Mass flow rate is an independent variable in the screening analysis only. Set out in Table 1, data handled in this thesis is divided into two groups: geothermal energy source (reservoir and contained fluid) conditions, and project (operating) conditions.

Geothermal energy source		**Project**
Reservoir	**Fluid**	**Operational**
Depth, z (m)	Temperature, T (^{o}C)	CPG plant type
Temperature, T (^{o}C)	Pressure, P (MPa)	Well diameter, D (m), spacing, L (m), and friction factor, f
Thickness, b (m)	Specific enthalpy, h (kJ/kg)	Turbine isentropic efficiency
Permeability, k (mD)	Density, ρ (kg/m^3)	Heat exchanger variables
Hydrostatic pressure (MPa)	Specific entropy, s (kJ/ (kg k))	Mass flow rate, M (kg/s)
	Dynamic viscosity, μ (Pa S)	

Table 1: Reservoir, fluid, and operating conditions used to estimate CPG power generation

Reservoir data for gas fields in the SNS are sourced from Geological Society Memoir 52 (Goffey and Gluyas, 2020). Appendix A from the memoir references of an exhaustive list of papers on UK oil and gas fields, including abandoned, producing, and undeveloped fields. Included in these papers is information from field exploration and development history to reservoir structure and seismic interpretation. Trap, main pay zone, hydrocarbons, formation water, reservoir conditions, field size, and production data are also usually tabulated, altogether summarising the current subsurface understanding of many fields. Papers for 64

out of 145 SNS gas fields (including some field groups of the same name) contain complete data for the purpose of estimating CPG power production. For the remaining fields, some papers either do not include all the necessary data, or include temperature and depth as ranges only, and some do not have a published paper. Where reservoir permeability and thickness are given as a range, mean values are used. Initial reservoir pressure is assumed as equivalent to the hydrostatic pressure at that reservoir depth, although initial pressure values are published in the SNS gas field papers. Since pressure decreases as gas is produced and is recovered as the reservoir is injected with CO_2, initial pressure for CPG can be engineered to some degree. Using hydrostatic pressure allows fields of different depths and geothermal gradients to be compared to one another when initially selecting a target field (Section 4).

Reservoir conditions depth and temperature dictate the initial CO_2 fluid 'state' from which a CPG thermodynamic cycle can be constructed and solved for power generation. When considering the thermosiphon effect and frictional losses throughout the CPG system in the main analysis (Section 5), reservoir thickness and permeability, in addition to well diameter (operational) conditions, are applied.

'CPG plant type' refers to whether the power cycle is direct or indirect. Direct systems are exclusively analysed in this study, meaning heated CO_2 is directly expanded through a turbine to generate power in the surface plant. The degree of this expansion is only so much that the fluid remains in the supercritical state. This differs from the direct CPG studies in the literature where the fluid is usually expanded below the critical point (7.4 MPa and 31 ^{o}C), thereby transitioning into the two-phase region. The effect of this difference on power production is discussed in Section 6.3. The use of the remaining operational conditions is justified in Sections 4 and 5.

4. Selecting a target field

In this screening analysis, an impracticable upper limit of direct CPG power generation is estimated for 64 SNS gas fields. By doing so, the most suitable geothermal energy source from which quantities may be recovered by the project, in terms of power generation potential and practicality, can be selected. Second-order controls are then applied in the main analysis (Section 5) to achieve a more accurate estimate of power generation for the selected field, so that the quantities can be reported and classified with higher confidence.

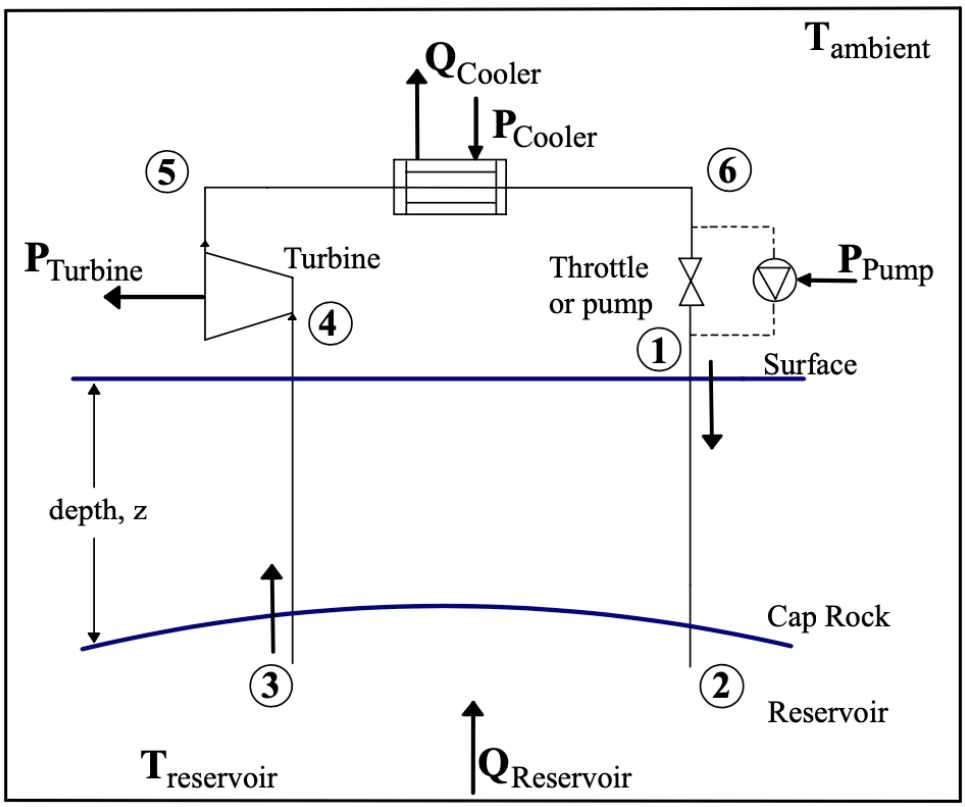

Fig.5: Direct CPG schematic diagram adapted from (Adams et al., 2021)

Figure 5 is representative of a direct CPG system which assumes quasi-static flow. For each field, the thermodynamic properties of CO_2 at each stage are progressively calculated from an initial known state, which is at the production well sandface (state 3). Here, the fluid is equivalent to the reservoir pressure and temperature. Specific enthalpy, specific entropy, and density are deduced by inputting these fluid temperature and pressure values into an online calculator (CO_2 Tables Calculator, 2021). This calculator uses an equation of state for carbon

dioxide published in (Span and Wagner, 2003), and a reference state (where the enthalpy and entropy of the ideal gas is set to zero) at 298.15 K and 0.101325 MPa.

The CO_2 fluid pressure at the turbine inlet (state 4), here assumed as equal to that at the production wellhead, is found by multiplying the effective fluid density in the well by the change in gravitational potential energy from state 3, which equals the pressure difference from state 3 to 4. This solution is derived from the Bernoulli equation and is explained in Section 5.1. Temperature at state 4 also decreases from state 3 as the fluid moves up the production well, since the increase in potential energy is balanced by a decrease in enthalpy in this assumed isentropic expansion process. With known pressure and entropy, the CO_2 fluid enthalpy and temperature values are deduced.

From states 4-5, CO_2 is expanded isentropically in a turbine down to 7.5 MPa to remain in the supercritical phase. Power generated by the direct turbine is the product of the difference of inlet and exit enthalpies multiplied by mass flow rate and the isentropic turbine efficiency (Equation 1). An arbitrarily chosen mass flow rate is fixed at 100 kg/s for each field, and an isentropic turbine efficiency of 80% is chosen after (Adams *et al*., 2015), which based on data from a manufacturer (Welch and Boyle, 2009).

$$\dot{P}_{turbine} = \dot{m} \cdot \eta_{turbine} \cdot (h_4 - h_5) \quad (1)$$

From states 5-6, CO_2 is cooled nearly-isobarically using a shell and tube heat exchanger. The heat exchanger has a counter flow arrangement with a single pass on both the tube-side and the shell-side. CO_2 passes on the tube-side to minimise the pressure drop, which is set to remain under 1 kPa. Seawater is pumped through the shell-side; the power required to do so is the parasitic load of the CPG system. Tubes are composed of carbon-steel with a thermal conductivity of 45 W/m.K in the non-fouled condition and the shell is assumed to be thermally isolated from the surroundings.

The difference between the seawater temperature (the sink) and the temperature at which the fluid is cooled to is referred to as the approach temperature, which is chosen to the nearest degree so that CO_2 reinjected at state 6 can be isentropically compressed to the reservoir hydrostatic pressure at state 2 (Adams *et al*., 2014) (Adams and Kuehn, 2012)

(Adams *et al*., 2021). A conservative choice of 8 °C for the average coolest accessible seawater is made, taking into account seasonal fluctuations and annual trends for the SNS at different depths (Morris et al., 2018). Once the required approach temperature has been established, both the inlet and the outlet temperatures of CO_2 on the tube-side are known. Since pressure is assumed to be constant (at 7.5 MPa), the specific enthalpy of CO_2 at the outlet (state 6) can be deduced. The change in enthalpy of CO_2 across the heat exchanger is multiplied by mass flow rate (100 kg/s) to determine the rate of heat transfer, Qc. A fixed mass flow rate of 200 kg/s is assumed for the shell-side to achieve a high heat transfer coefficient while maintaining a sufficiently low pressure drop to avoid excessive parasitic loads. With a known shell-side inlet temperature (8 °C), known Qc, and known mass flow rate, the specific heat formula can be rearranged to find the shell-side outlet temperature.

The required heat transfer surface area of the shell and tube heat exchanger specific to each gas field is found using Equation (2):

$$A_{required} = \frac{Qc}{U \cdot \Delta Tlm} \tag{2}$$

$$\Delta Tlm = \frac{(T_{hi} - T_{co}) - (T_{ho} - T_{ci})}{\ln\left(\frac{T_{hi} - T_{co}}{T_{ho} - T_{ci}}\right)} \tag{3}$$

The logarithmic mean temperature difference, ΔTlm, is found by inputting the inlet and outlet temperatures of both fluids into Equation (3). The bulk mean temperature and pressure of each fluid is entered into online calculators for CO_2 (CO_2 Tables Calculator, 2021) and seawater (Arain, 2021) (the seawater calculator is based off algorithms published by (Sharqawy *et al.*, 2010) and pressure is set to 0.1 MPa) to deduce additional thermophysical properties of each fluid. These properties are implemented in a set of simplifying relations described in Appendix C of (Smith, 2005) to find the overall heat transfer coefficient, U. U is a function of the two fluid's velocities, which in turn depend on the heat exchanger design (meaning the length and number of tubes). By changing the heat exchanger design, the actual heat transfer surface area changes. Considering the required area is a function of U (Equation 3), an iterative solution technique is thus used to find a heat exchanger design where the actual area and the required area are close to equal.

Pressure drops are quantified from the same set of relations described in Appendix C of (Smith, 2005), again using velocity as a bridge to relate the pressure drops to the respective film transfer coefficients on each side of the heat exchanger. Pumping power for the shell-side is found using Equation 4 where the pump efficiency is 0.6, ΔPs is the shell-side pressure drop, ρ is the mean density of seawater on shell-side, and $\dot{m}$ is 200 kg/s. Potential implications of the assumptions made for the proposed shell and tube heat exchanger design method on the CPG system are detailed in Section 6.2.2.

$$\dot{P}_{\text{seawater pump}} = \left(\dot{m} \cdot \frac{\Delta Ps}{\rho}\right) / \eta_{\text{seawater pump}} \tag{4}$$

Net power production is the difference between the turbine power output and the parasitic cooling load (Equation 5). The fluid is reinjected at state 1, which is identical to state 6 in a frictionless system. In a CPG system with friction, pressure losses occur as the CO_2 fluid moves through the pipes and reservoir. A surface pump may be added at the injection wellhead to overcome these pressure losses and generate flow. Since the CPG system is assumed to be frictionless in this section, there are no parasitic pumping requirements, and a mass flow rate is simply selected. Similarly, the thermosiphon effect is discounted. The SNS fields screened for this study and corresponding calculations are set out in the appendix.

$$\dot{P}_{\text{net}} = \dot{P}_{\text{turbine}} - \dot{P}_{\text{seawater pump}} - \cancel{\dot{P}_{\text{surface pump}}} \tag{5}$$

A target field is now selected for further analysis in Section 5. This field is estimated to be the most suitable geothermal energy source from which quantities may be recovered by the project, in terms of power generation potential and practicality.

Net power generation, together with the respective shell and tube heat exchanger surface area needed to achieve that power generation, are shown for 50 SNS gas fields in Figure 6. Notably, only every fourth field is labelled on the x-axis. Fourteen fields were found to have reservoirs that are too shallow to be considered for the supercritical CPG system proposed in this study. This is because the CO_2 fluid pressure drops below the critical point by the time it reaches the production wellhead, meaning it enters the turbine inlet already in the two-phase region. The mean net power output of the 50 working fields is 449 kWe, ranging from 58 - 930 kWe. Likewise, the mean heat exchanger surface area is 1009 m^2, ranging from

132 - 3,310 m^2. In design terms, 132 m^2 equates to a 0.4 m shell diameter with 2.5 m long tubes, whereas a 1.9 m shell diameter with 14 m long tubes is needed to cover 3,310 m^2. Thus, considering the congested nature of offshore platforms, heat exchanger surface area is established as a practical measure for selecting a target field. A conservative upper limit (in practicality terms) of 500 m^2 (the Tolmount Field and below) is chosen to ensure the heat exchanger dimensions are within a suitable range for integration with an existing platform.

Fig. 6: Net power generation and heat exchanger surface area for 50 SNS gas fields in a 100 kg/s frictionless CPG scenario

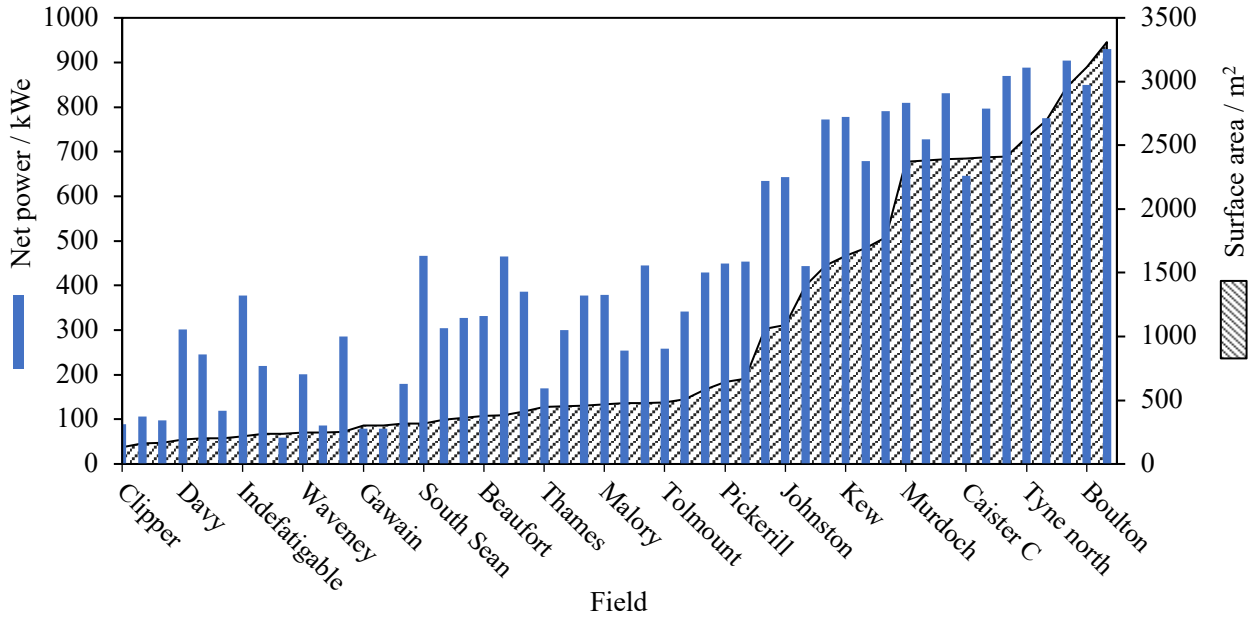

Fig. 7: The relationship between required heat exchanger surface area and reservoir depth for 50 SNS gas fields in a 100 kg/s frictionless CPG scenario

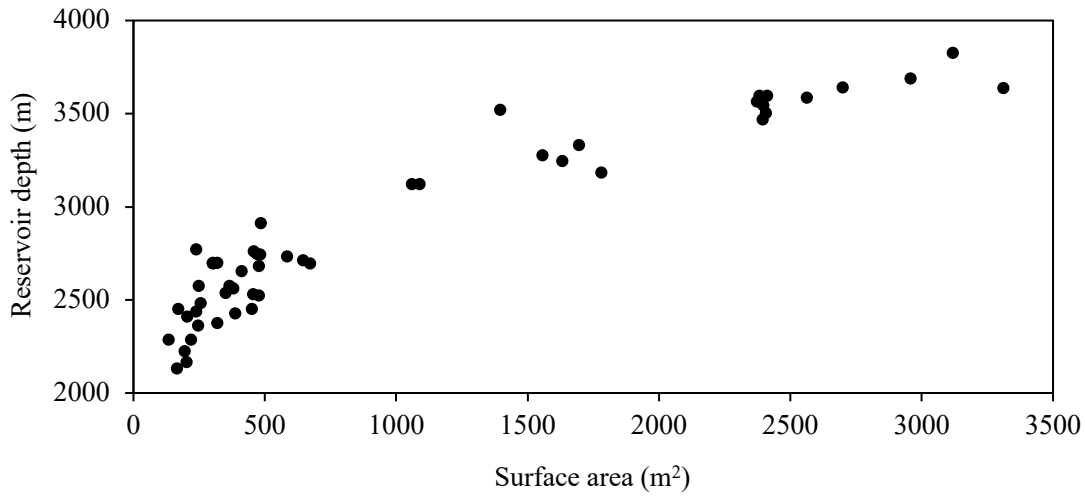

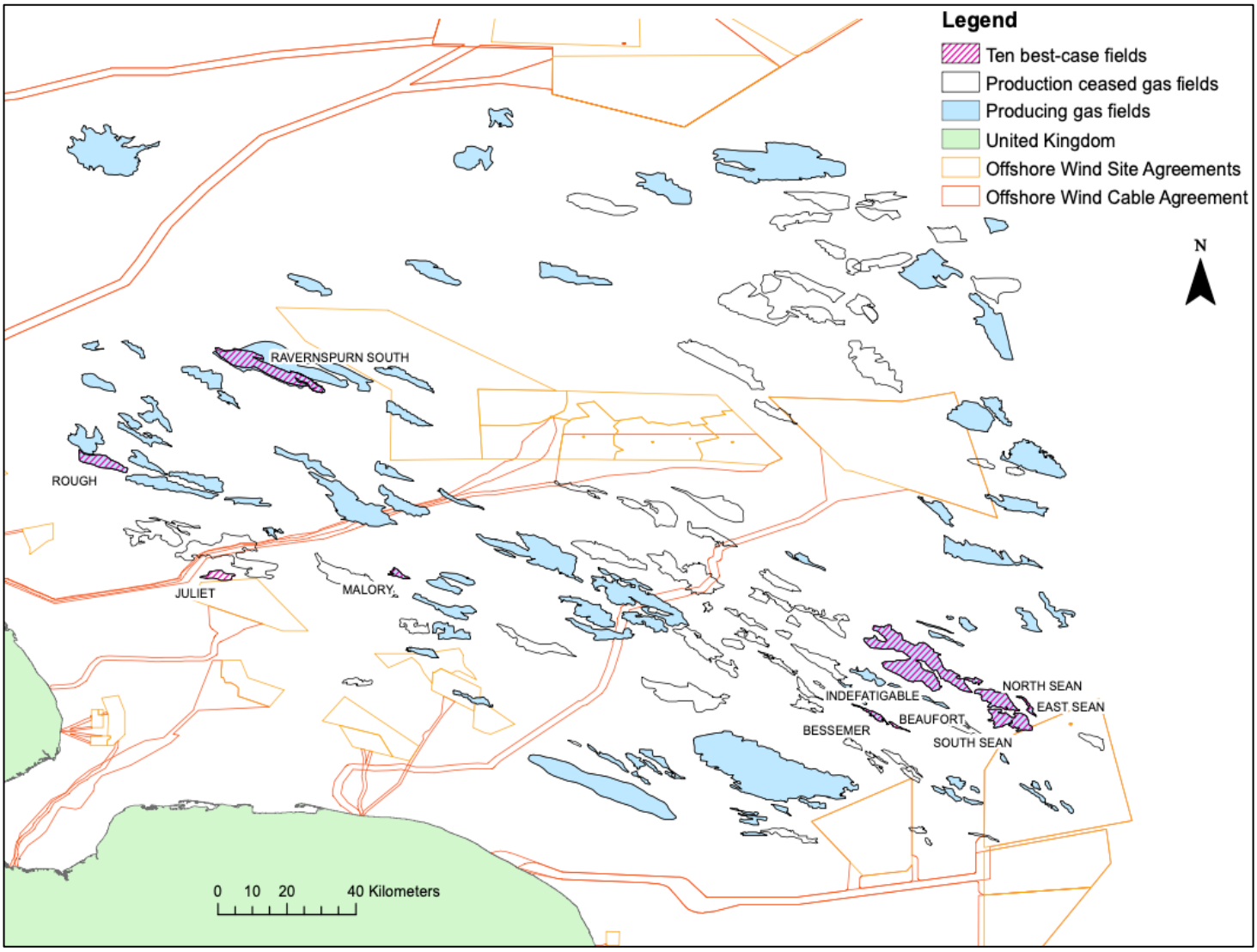

Fig. 8: Map to show the ten best-case SNS gas fields in a frictionless direct CPG scenario

Figure 8 shows a map of the ten best-case SNS gas fields in a direct CPG scenario after applying heat exchange surface area as a practicality constraint, based off net power generation values. Of these fields, South Sean can produce the most power (466 kWe) and is selected as the target field for further analysis in Section 5. This selection is discussed further in Section 6.3, along with the potential drawbacks of the method used in this section.

5. The South Sean Field analysis

The thermosiphon effect, as well as the frictional pressure drop that occurs as CO_2 moves through the wells and reservoir, are considered in this section to estimate power generation for the South Sean field with improved accuracy. The effects of varying well diameter on power generation are investigated in addition to the base case. Table 2 summarises the reservoir conditions and base case well conditions for South Sean.

Depth to crest (m)	2377.4
Gross thickness, *b*, (m)	77.7
Permeability, *k*, (mD)	600
Temperature, *T*, (°C)	94.4
Initial pressure, *P*, (MPa)	23.77
Well configuration	Injection-production well doublet
Well diameter, *D*, (m)	0.14
Well spacing, *L*, (m)	707

Table 2: South Sean reservoir conditions (Botman and van Lier, 2020) and base case well conditions

As established in the prior screening analysis, the CO_2 fluid is injected at state 1 (Figure 5), moving nearly-isentropically to state 2. By state 3 the fluid has heated to the reservoir temperature (94.4 ºC) and decreased to the reservoir hydrostatic pressure (23.77 MPa) at a depth of 2.38 km. Plotted on a Mollier chart (Figure 9), sCO_2 at 94.4 ºC follows the line of constant entropy up the production well from 23.77 MPa to 9.91 MPa, yielding a temperature of 47.3 ºC at state 4. From states 4-5, the fluid is isentropically expanded through a turbine to 7.5 MPa to remain in the supercritical phase. From states 5-1, the fluid is cooled isobarically so that it can be isentropically compressed to the reservoir hydrostatic pressure at state 2. Notably, the entropy and enthalpy values shown on the Mollier chart have a different reference state to the values in Table 3, which shows the thermodynamic properties of the CO_2 fluid at each state in the cycle.

	State				
Property	(3)	(4)	(5)	(6/1)	(2)
Pressure (MPa)	23.77	9.91	7.50	7.50	24.14
Temperature (°C)	94.4	47.3	32.1	28.0	52.7
Specific enthalpy (kJ/kg)	-110.85	-137.53	-143.63	-227.92	-206.34
Density (kg/m^3)	594.30	424.48	365.19	713.55	813.67
Specific entropy (kJ/(kg k))	-1.20480	-1.20480	-1.20480	-1.48185	-1.48185

Table 3: Thermodynamic properties of CO_2 at each state in the South Sean direct CPG cycle

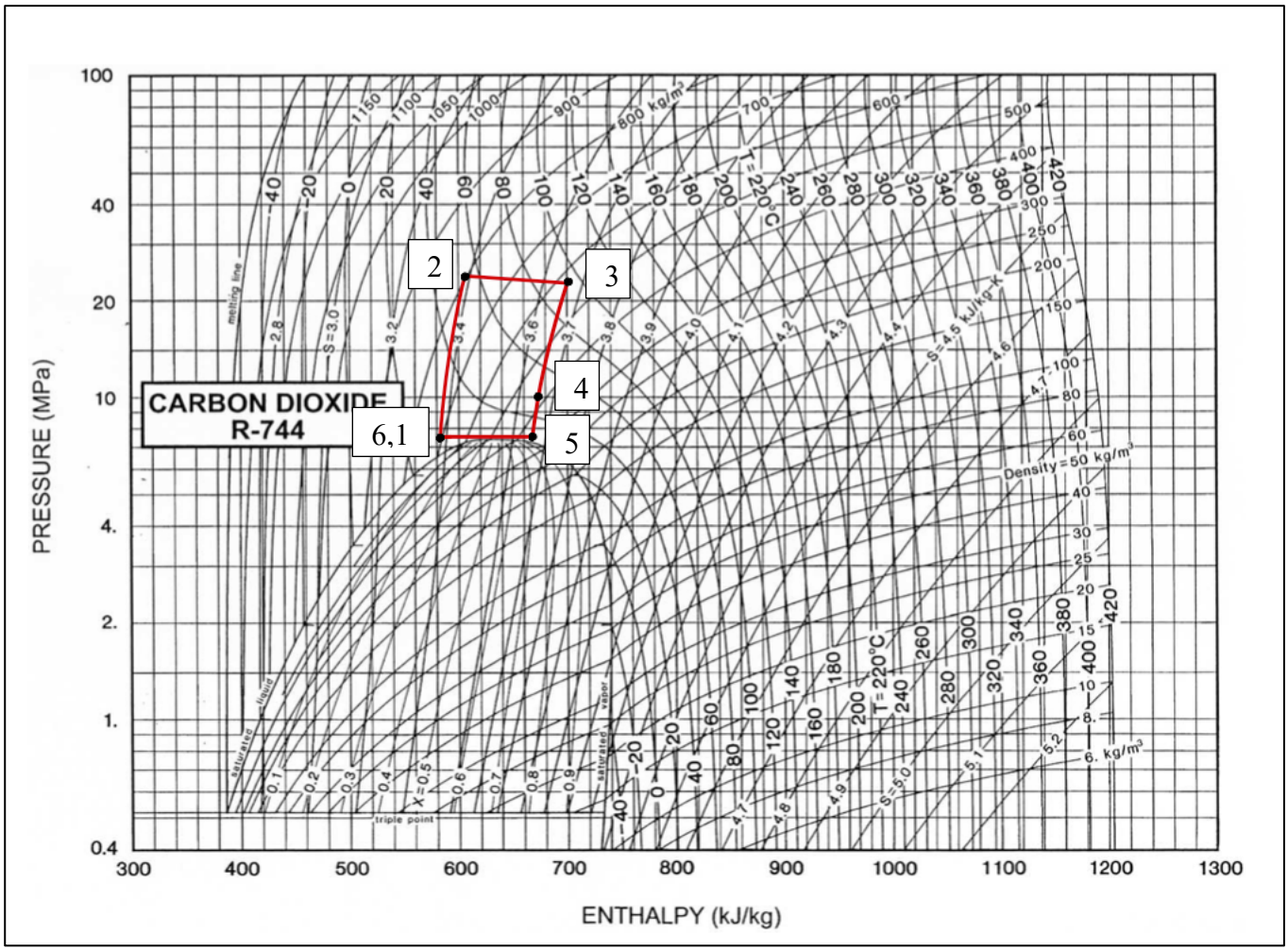

Fig. 9: Mollier chart to show the South Sean direct CPG cycle (ASHRAE handbook, 2010)

5.1 Estimating the thermosiphon-generated mass flow rate

The thermosiphon-generated mass flow rate is the rate at which the CO_2 fluid can self-circulate through a CPG system, which is used in the process of determining power generation (Section 5.2). The thermosiphon is driven by a pressure difference between the injection and production wellheads, which occurs because the effective densities of CO_2 are different in each well. This can be explained using Equation (6), as set out in (Adams *et al*., 2021), which is derived from the Bernoulli equation:

$$\eta \int \frac{\Delta P}{\rho} = \int \Delta h + Q_{loss} \quad (6)$$

Work done from states 1-2 or 3-4 in Figure 5 is equal to the change in enthalpy between well inlet and exit, less heat losses. The change in enthalpy, Δh, is fixed to gravitational potential energy (neglecting the effects of kinetic energy):

$$\begin{aligned} \Delta h &= g\,(\Delta z) \\ &= 9.81\ m/s^2 * 2377.4\ m \\ &= 23323\ m^2/s^2 = 23.32\ kJ/kg \end{aligned}$$

η is the isentropic efficiency to account for non-ideal pressure losses within the well: pressure decreases up the production well due to an increase in elevation, and pressure losses accumulate due to friction with the pipe wall (Adams *et al*., 2014). For a quasi-static fluid (frictionless / $\eta = 1$) there are no pressure losses, and assuming the wells are adiabatic ($Q_{loss} = 0$), the change in pressure between the entrance and the exit of a well (ΔP) is therefore a function of wellbore fluid density (ρ):

$$\int \frac{\Delta P}{\rho} = 23.32\ kJ/kg$$

In a real system, CO_2 density is dependent on temperature and pressure, which vary across each well. In a simplification, this analysis assumes an effective fluid density (a single density value across the whole well), $\bar{\rho}$, for both the injection and production wells. $\bar{\rho}$ for the injection well is assumed to be the density of that which is injected at state 1, and $\bar{\rho}$ for the

production well is assumed to be the same as the density of CO_2 that has increased to reservoir temperature and pressure (state 3, at the sandface). $\bar{\rho}$ in the injection well is higher than $\bar{\rho}$ in the production well because this CO_2 has been cooled, so the change in pressure between a well inlet and exit (ΔP) is greater for the injection well. Assuming both well-bottoms are equivalent to the reservoir hydrostatic pressure (state 3) or just above (state 2), a resultant excess pressure occurs at the production wellhead (state 4), known as the thermosiphon-generated pressure difference, ΔP_{ts} (Adams *et al*., 2021). The effective fluid densities of each well are found using the online calculator referenced in Section 4 (CO_2 Tables Calculator, 2021). The output values were initially confirmed using a pressure-enthalpy chart (ASHRAE handbook, 2010) and lookup table (Span and Wagner, 1996) for CO_2. ΔP_{ts} is calculated in Equations (7) to (10):

- Production wellhead pressure (state 4): 594.30 kg/m^3 · 23.32 kJ/kg = 13.86 MPa

  23.77 MPa (reservoir pressure) – 13.86 = 9.91 MPa (7)

- Injection wellhead pressure (state 1): 713.55 kg/m^3 · 23.32 kJ/kg = 16.64 MPa

  24.14 MPa – 16.64 = 7.50 MPa (8)

- Thermosiphon-generated pressure difference: 9.91 – 7.50 = 2.41 MPa (9)

A thermosiphon-generated pressure difference of 2.41 MPa can circulate CO_2 through the reservoir and wells at a certain mass flow rate, $\dot{m}$. ΔP_{ts}, along with any additional pump pressure differences, $\Delta P_{pumping}$, reaches equilibrium with the sum of the wellbore and reservoir pressure losses, ΔP_{losses} , as shown in Equation (10) (Adams *et al*., 2021):

$$\Delta P_{ts} + \Delta P_{pumping} = \Delta P_{losses} \quad (10)$$

For an unpumped, or thermosiphon-only system, $\Delta P_{pumping}$ can be neglected. ΔP_{losses} are made up of both pipe pressure losses and reservoir pressure losses, which occur as CO_2 circulates through the system. Surface losses are not included in this part of the analysis as there is minimal piping at the surface. Pipe pressure losses increase with mass flow rate

squared (Darcy-Weisbach equation) (Adams *et al*., 2015) and reservoir pressure losses increase linearly with mass flow rate (Darcy equation) (Adams *et al*., 2021(b)):

$$\Delta P_{pipe} = f \cdot \frac{2z}{D^5} \cdot \frac{8}{\pi^2} \cdot \frac{1}{\rho} \cdot \dot{m}^2 \quad (11)$$

$$\Delta P_{pipe} = 0.02 \cdot \frac{2\,(2480.3\text{ m})}{14\text{ cm}^5} \cdot \frac{8}{\pi^2} \cdot \frac{1}{653.9\text{ kg/m}^3} \cdot \dot{m}^2$$

$$\Delta P_{pipe} = (0.0023) \cdot \dot{m}^2$$

$$\Delta P_{reservoir} = \frac{\mu}{\rho} \cdot \frac{1}{k \cdot b} \cdot \frac{1}{\pi} \cdot \ln\left(\frac{L}{D \cdot e}\right) \cdot \dot{m} \quad (12)$$

$$\Delta P_{reservoir} = \frac{4.67 \times 10^{-5}\text{ Pa s}}{589.43\text{ kg/m}^3} \cdot \frac{1}{600\text{ mD x }77.7\text{ m}} \cdot \frac{1}{\pi} \cdot \ln\left(\frac{707\text{ m}}{0.14\text{ m x }e}\right) \cdot \dot{m}$$

$$\Delta P_{reservoir} = (0.0013) \cdot \dot{m}$$

The friction factor, *f*, used in the Darcy-Weisbach Equation (11) follows that used by (Adams *et al*., 2015), which was established using a Moody Chart with a pipe surface roughness of 55 μm. This roughness is conservatively high for standard oil and gas steel piping designed for corrosive environments (Farshad and Rieke, 2006). Wells are drilled at an angle from a single location at the surface (mean sea level) to reach reservoir depth, 707 m apart. Therefore, pipe length, *z*, is equal to $((2377.44^2 + 707^2)^{0.5})$. Pipe diameter, D, is 14 cm in the base case. Density in Equation (11) is the average of the injection well and production well effective densities.

Dynamic viscosity, μ, used in the Darcy Equation (12) is estimated from explicit correlations published in (Ouyang, 2011) to calculate μ under operational conditions anticipated for a CCS project. *k* and *b* are the permeability and average thickness of the reservoir. Density of CO_2 in the reservoir is approximately the average of states 2 and 3 (Table 3). It is also noted that in Equation (12), 1mD-m equals 10E-15 m^3

The combined reservoir and pipe frictional pressure drop is plotted against mass flow rate in Figure 10 to find the mass flow rate generated by a thermosiphon-generated pressure difference of 2.41 MPa. This is equivalent to the maximum thermosiphon-generated mass flow rate.

Fig.10: Mass flow rate vs. total pressure losses for the South Sean direct CPG system

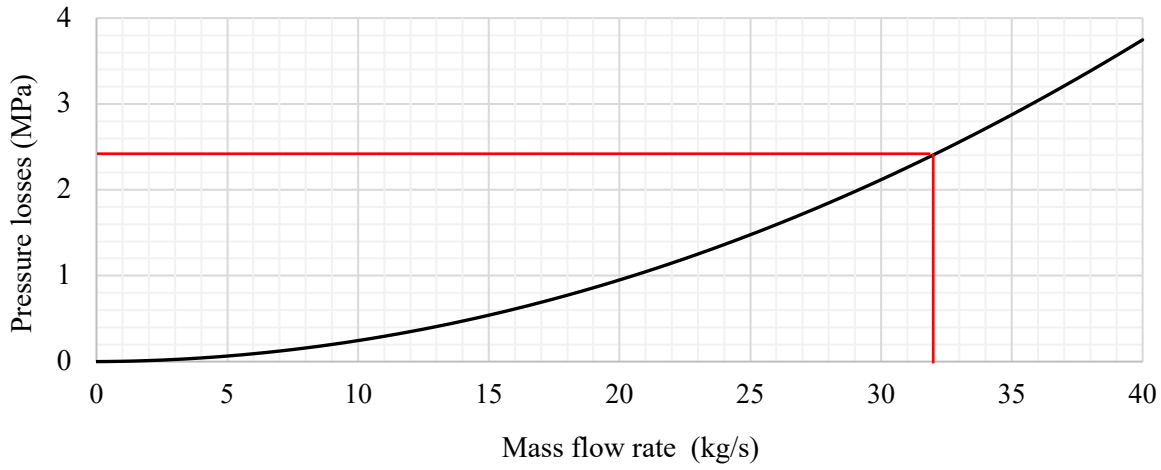

$$\Delta P_{ts} = \Delta P_{losses}$$

2.41 MPa = 32 kg/s (thermosiphon-generated mass flow rate)

5.2 Estimating power generation

In accordance with the method used for selecting a target field (Section 4), net power production is the difference between the turbine power output and the parasitic cooling load (Equation 5). However, to estimate net power generation for a direct CPG system that takes friction into account, an alternative method is used to calculate the turbine power output. This method accounts for the pressure losses incurring in the piping and reservoir that increase with mass flow rate (Figure 10). The sum of these losses is effectively subtracted from the turbine inlet pressure, in turn, decreasing the change in enthalpy across the turbine.

$$\dot{P}_{turbine} = \dot{m} \cdot \eta Turbine \cdot \frac{\Delta P}{\bar{\rho}} \quad (13)$$

The turbine power output is the product of mass flow rate, the turbine isentropic efficiency, the pressure difference across the turbine, and the effective fluid density (Equation 13) (Adams *et al*., 2015). One portion of the thermosiphon-generated pressure difference can be used to circulate CO_2 ($\dot{m}$) and the other portion can be used to generate power (ΔP). A throttle valve is set up at state 1 (Figure 5) to achieve the desired pressure drop and mass flow rate combination. The effective fluid density is calculated as the average of the turbine inlet and outlet densities.

Fig.11: Optimising turbine power output in the South Sean direct CPG system

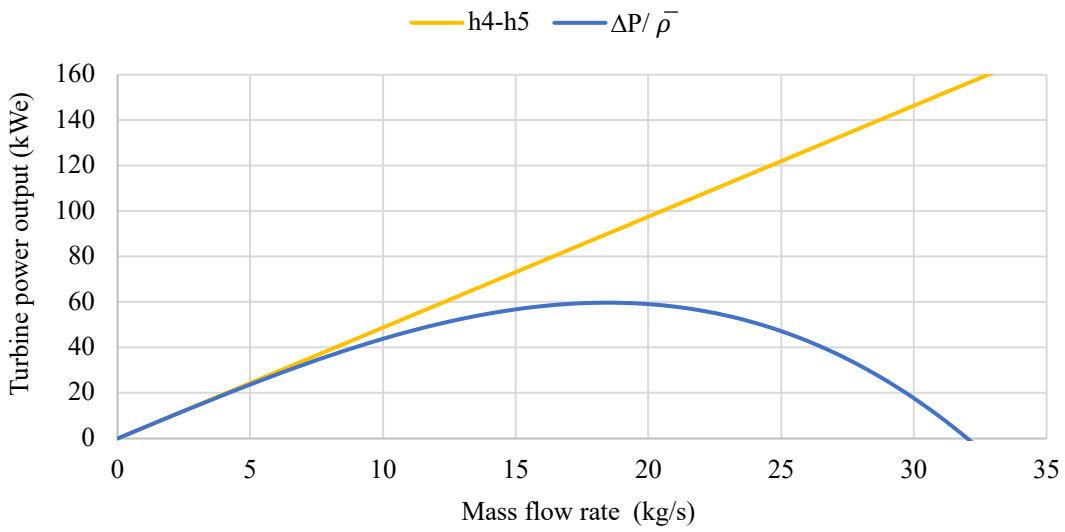

Figure 11 compares the use of Equations (1) and (13) for determining the net power output of the system. Equation (1), represented by 'h4 - h5' (the enthalpy difference across the turbine), indicates that power produced by the turbine increases linearly with mass flow rate. While Equation (13) ($\Delta P/ \bar{\rho}$) is also used to determine power produced by the turbine, it considers the frictional pressure drop that occurs CO_2 circulates around the system; as more of the thermosiphon-generated pressure difference is used to circulate CO_2 at increasing mass flow rates, the pressure difference across the turbine (and the consequent turbine output) decreases. Therefore, a mass flow rate of 18 kg/s is selected to maximise turbine power production at 59.71 kWe for the base-case. The turbine power generation calculation is set out following Equation (13):

$$\dot{P}_{turbine} = 18\ kg/s \cdot 0.8 \cdot \left(\frac{1.64\ MPa}{((424.48 + 365.19\ kg/m^3)/2)}\right) = 59.71\ kWe$$

Equation (4) from Section 4 is used to estimate the power required to circulate seawater around the shell-side of the heat exchanger to cool CO_2 prior to reinjection, and Equation (5) is used to calculate net power production:

$$\dot{P}_{cooling\ pump} = \left(36\ kg/s \cdot \frac{7355.16\ Pa}{1026.38\ kg/m^3}\right) / 0.6 = 0.43\ kWe$$

$$\dot{P}_{net} = \dot{P}_{turbine} - \dot{P}_{cooling\ pump} = 59.28\ kWe$$

59.28 kWe can be generated using the base-case direct CPG system configured to the South Sean field. In certain CPG scenarios, a surface pump can be added at state 1 (Figure 5) to circulate CO_2 in addition to the thermosiphon-generated pressure difference to increase net power generation of the system. In this case, the additional parasitic losses associated with a surface pump would exceed the increase in net power generation, so no pump is used.

The overall heat/energy balance is presented below, along with the thermal efficiency and Carnot efficiency of the heat engine.

Qh = m*Δh = 18 * (-206.34 - -110.85) = (-)1718.82 kJ
Qc = 18 * (-143.63 - -227.92) = 1517.22 kJ
W (theoretical maximum work done by heat engine) = Qh – Qc = 201.60 kJ
Thermal efficiency = W/Qh = 11.73 %

$$\eta_{Carnot} = 1 - \left(\frac{T_C}{T_H}\right) = 1 - \left(\frac{(8 + 273.15)}{(94.44 + 273.15)}\right) = 23.52\ \%$$

5.3 The effect of well diameter on power generation

The base-case CPG system proposed for the South Sean field can be configured to generate more power by increasing the wells' diameters, since pressure losses in the well are inversely proportional to the fifth power of the well inner diameter (Equation 11), and reservoir pressure losses are inversely proportional to inner well diameter (Equation 12). This means the thermosiphon-generated mass flow rate increases with a larger well diameter while the pressure difference across the turbine (ΔP_{ts}) remains the same and so more power is generated by the turbine. Table 4 compares three well diameters and the respective power generation observed in what is otherwise the same CPG configuration. A diameter of 0.14 m is used in the base-case analysis (Section 5). A diameter of 0.41 m is typical of conventional geothermal systems at the South Sean reservoir depth (Finger and Blankenship, 2010). By way of comparison, 0.28 m represents the middle ground between these two diameters. These results are considered in Section 6.

Well diameter (m)	Mass flow rate (kg/s)	Turbine output (kWe)	Parasitic cooling load (kWe)	Net power (kWe)
0.14	18	59.71	0.43	59.28
0.28	101	320.11	21.41	298.70
0.41	247	766.97	214.89	552.08

Table 4: The effect of well inner diameter on the optimum mass flow rate and power production of a thermosiphon-based direct CPG system

6. Discussion

6.1 Classifying SNS gas fields as geothermal resources in the context of direct CPG

Following the resource classification process set out in the methodology (Section 3), the project and associated geothermal source have first been defined as a direct CPG system and the thermal energy contained in CO_2-filled SNS gas field reservoirs, respectively. In Sections 4 and 5, the geothermal energy product (defined as electrical power) is then quantified in different ways; in Section 4, an impracticable upper limit of power generation is estimated for gas 50 fields. In Section 5, the South Sean field is chosen as the best-case geothermal source and power generation is re-estimated whilst considering frictional pressure losses in the reservoir and wells that increase with the thermosiphon-generated mass flow rate. Finally, in this section, UNFC criteria (ECE, 2013) are used to classify the SNS gas fields as geothermal resources to complete the resource classification process.

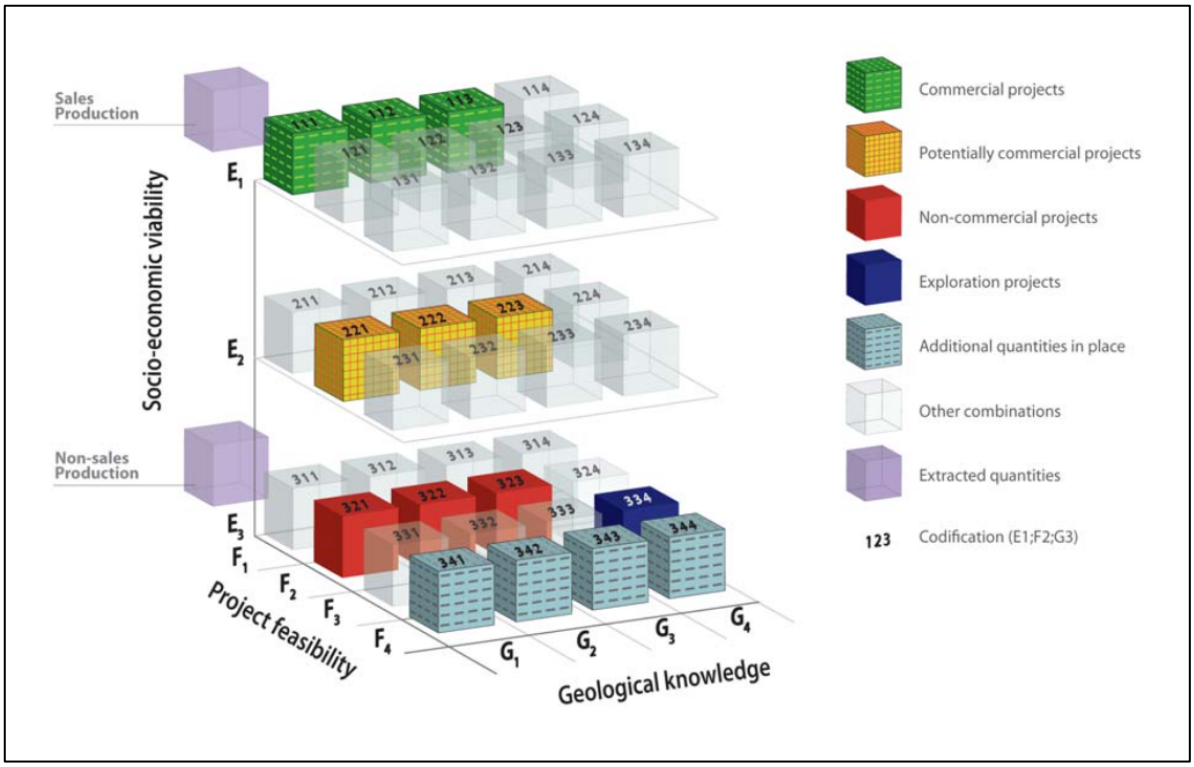

Figure 12: UNFC-2009 categories and examples of classes (ECE, 2013)

South Sean is firstly classified as a geothermal resource in a direct CPG scenario. To do so, categories and subcategories are defined for three UNFC criteria, and these criteria are combined to form a class. Figure 12 shows a three-dimensional class system created by different combinations of the criteria.

Socio-economic viability, criterion E, reflects the impact of socio-economic conditions on implementing the project at a commercial scale. For the base case, a maximum of 59 kWe can be generated by direct CPG, and this value increases to 552 kWe once the wells' diameters are increased to 0.41 m. To know whether the latter of these values is great enough to deem the project economically viable requires further analysis, which is beyond the scope of this study. Socio-economic factors considered in such an analysis should incorporate market prices along with regulatory, legal, contractual, and environmental conditions. Capital costs in this case include well retrofitting and/or drilling in addition to establishing a surface plant, and the operation and maintenance of the project. Thermal depletion of the reservoir due to the continuous re-injection of cooled CO_2 should also be considered to estimate potential revenue generated by the sale of the electricity over time. Furthermore, an energy penalty for CCS incurs before CPG heat extraction can begin which reduces the overall economic favourability of the project. Nonetheless, South Sean is situated at the border of a windfarm site agreement (Figure 8), so means of transmission could be available to meet onshore demand if the project was found to be economical. Consequently, South Sean as a potential geothermal resource for extraction via a direct CPG project falls under category/subcategory E3.3: 'there are not reasonable prospects for economic extraction and sale in the foreseeable future'. The evaluation is at too early a stage to determine economic viability.

The F criterion considers project feasibility based on the maturity of studies and any further undertakings requisite to a commercially operating project. CPG is a technology that is still under development and is yet to be demonstrated as technically viable for a geothermal energy source analogous to offshore gas fields. One field scale demonstration in 2015 proved the circulation of geologically stored CO_2 between a sedimentary reservoir and the surface (Freifeld *et al*., 2016), however, the test did not generate a steady non-zero thermosiphon-generated mass flow rate nor was a direct-fired turbine trialled. (Adams *et al*., 2021) postulate that liquid loading in the production well led to this unexpected result. At the time of writing, no known full pilot projects are being planned to demonstrate the viability of the technology.

Consequently, the project is classified on the F-axis as F4. This category is defined as ‘no development or mining project has been identified’. Specifically, the technology to recover the estimated quantities is currently being researched but no successful pilot studies have been completed (subcategory 4.2).

Categories of the G criterion (geological knowledge) rank the level of confidence in the potential recoverability of the estimated geothermal energy resource quantities. A combination of G categories is chosen to account for the full range of possible outcomes. For South Sean, ‘quantities associated with a known deposit can be estimated with a moderate to high level of confidence’, placing it in categories G1+G2. Both geological and geographical factors are considered to justify this choice. The South Sean reservoir data (depth, temperature, thickness, and permeability) used in the second analysis of this study are the result of direct measurements, meaning they have a high associated level of confidence. However, they do not reflect the reservoir as a whole and different uncertainties remain. These uncertainties primarily relate to the geothermal energy source and are addressed in Section 6.2.3.

A class is now defined from the categories/subcategories established for South Sean as a geothermal resource in a direct CPG scenario. E3.3, F4.2 and G1+G2, or simply ‘342’, equates to the class ‘additional quantities in place associated known deposits’. The estimated quantities are not recoverable by the currently defined project, although a portion of these quantities may become recoverable in the future.

The forty-nine remaining fields found to be net positive for direct CPG in Section 4 are not considered in economic viability terms, similarly to South Sean. Therefore, the reported quantities for these fields must also be classified as F4, having ‘additional quantities in place associated known deposits’. Fourteen fields initially considered in this study have reservoirs that are too shallow to enable CO_2 to be expanded through the turbine in its supercritical state. With no discernible geothermal energy product, a class cannot be defined for these fields.

6.2 Critical review of the study design

Several principal assumptions were introduced in Sections 4 and 5 both to simplify the process of estimating power generation in different ways and to select the best-case SNS gas field for direct CPG, all the while remaining within the constraints of this study. The aim of this section is to clarify and justify these assumptions, reviewing the design of this study in doing so.

6.2.1 Wellbore calculations

The direct CPG thermodynamic cycle was solely constructed upon the known CO_2 fluid state at the sandface in the production well. To derive the CO_2 fluid state at the production wellhead, several assumptions were made to satisfy Equation 6, including adiabatic conditions from well bottom to wellhead, the omission of kinetic energy effects, and the application of a single effective density value throughout the well.

Of the 3 wellbore calculation assumptions outlined above, allocating the known CO_2 density value at the production well sandface to the effective density value throughout the well is the most impactful on the wellhead fluid state, and consequently the net power output of the CPG system. This was done to simplify the calculation procedure in a repeatable way for the multiple gas fields considered in the analyses. The CO_2 fluid expands as it rises in the production well, becoming less dense with decreasing temperature and pressure. However, the rate of this decrease in density is inconstant (shown by the integral in Equation 6). For this reason, the actual mean density in the well cannot be easily calculated and the effective density is used to determine both the change in pressure from well bottom to wellhead and the resultant wellhead state since the expansion is isentropic. Furthermore, since density decreases up the production well, the effective density over-estimates the actual mean density, thereby over-estimating the change in pressure. In other words, the thermosiphon-generated pressure difference and the net power output of the CPG system are under-estimated by using the effective density. This drawback can be resolved to some degree by dividing the well into several increments then implementing an iterative solution technique. In this way, the change in pressure from well bottom to wellhead (or vice versa in the case of

the injection well) is calculated recursively from a level nΔz to (n+1)Δz by assigning $P_{n+1} = P_n + \rho g \Delta z$ (Pruess, 2006). The well depth z is divided into N increments and so $\Delta z = z/N$. This solution is demonstrated in the appendix, indicating around a 50% increase in turbine power output for the South Sean CPG system. Moreover, using this solution increases the approach temperature required to isentropically compress CO_2 down the injection well, decreasing the shell and tube heat exchanger size as a result. In (Randolph *et al*., 2012) and various subsequent studies on CPG performance by the same authors, Engineering Equation Solver (EES) is used to compute similar solutions for wellbore flow. EES is a simultaneous equation solver with in-built thermodynamic property data, allowing for the application of this solution to a range of CPG systems with varying reservoir temperatures and depths.

The wells are assumed to be adiabatic in this study, meaning no heat is lost to the surroundings from well bottom to wellhead and vice versa. This assumption holds strong for many CPG studies in the literature due to the low thermal conductivity of the surrounding rock. However, in an offshore setting, CO_2 must pass through a riser surrounded by seawater which is up to around 50 m deep in the SNS (Morris *et al*., 2018). This could lead to convective heat transfer and consequently a decrease in the net power output of the CPG system. In this case, piping near the surface should be thermally insulated as a mitigation strategy.

Changes in kinetic energy occur as CO_2 passes through the wells, however, any potential effects of these changes are discounted in this study. Based off the iterative solution demonstration for the South Sean wells, velocity in the production well changes from 10.9 to 14.4 m/s. This equates to a kinetic energy change of 588 J, or 2.5% of the total energy change from well bottom to wellhead. This small energy change would have a minimal impact on the net power output of the CPG system, especially when compared to the effective density value assumption.

6.2.2 Shell and tube heat exchanger calculations

Several main assumptions were made in the analyses to simplify the shell and tube heat exchanger calculations, thereby making them easily applicable across a range of fields with

reservoirs of varying depth and temperature. These assumptions are presented subsequently, along with any potential impacts they might have on the CPG system and its performance.

First, the temperature of seawater entering the shell-side is conservatively assumed be constant at 8ºC. That said, the shallow nature of the SNS (mostly >50 m in depth) means that temperature is sensitive to variations in the weather. Additionally, during the winter months, the shallow waters in the SNS are furthest from the inflowing waters of the North Atlantic and so they tend to be the coolest of the greater North Sea area. Conversely, water at the surface is warmer than water found towards the seabed during the summer months (Morris *et al*., 2018). Seawater is the heat sink which crucially dictates the thermal efficiency of the heat engine. Hence, as the seawater temperature fluctuates, mass flow rate on the shell-side must be adjusted accordingly for heat rejection to remain constant. For example, mass flow rate on the shell-side may need to increase during the warmest months, augmenting the parasitic load in doing so.

Secondly, the use of the logarithmic mean temperature difference (Equation 3) to determine the required heat transfer surface area of the heat exchanger specific to each gas field (Equation 2) may overpredict the actual mean temperature difference between each side of the heat exchanger, underestimating the required heat transfer surface area and the overall heat transfer coefficient as a result. The specific heat capacity of CO_2 on the tube-side increases substantially around the critical point, which falls within the operating range of the heat exchanger. This results in a non-linear rise in temperature from the inlet to the outlet. On the other hand, the specific heat capacity of seawater on the shell-side is almost constant and so its temperature rises steadily. Consequently, a 'pinching' effect may occur, where the temperature difference between the fluids at the ends is greater than in the middle of the heat exchanger. (Chen, 2016) conducted a pinch point analysis for a counter flow tube-in-tube heat exchanger model. sCO_2 was cooled below the critical point using water and the effect of several heat exchanger design variables on the pinch point position was determined. The actual mean temperature difference was derived from calculated conductance values (overall heat transfer coefficient, U, multiplied by heat transfer surface area) by splitting the heat exchanger into many segments. The actual mean temperature difference was then compared with the LMTD, finding that the heat exchanger may be undersized by up to 60 % when using the LMTD. However, the CO_2 was cooled over a much greater temperature range (from 100ºC) and at much lower mass flow rates (from 0.015 kg/s) compared with this study.

Therefore, the heat exchanger designs in this study may not be as significantly undersized as 60%. In any case, the heat transfer surface area for the South Sean base case is just 161 m^2 - around 30% of the 500 m^2 proposed practical limit.

Lastly, to sufficiently cool CO_2 in the surface plant prior to re-injection into the reservoir, the mass flow rate of seawater on the shell-side of the heat exchanger was fixed to 200 kg/s regardless of variations in approach temperature from field to field. This assumption was made so that working heat exchanger designs specific to each field could be devised with relative ease. By increasing the shell-side mass flow rate beyond 200 kg/s, the shell-side outlet temperature decreases according to specific heat formula. With a decreased shell-side outlet temperature, the LMTD increases. Furthermore, increasing the shell-side mass flow rate increases U. With an increased LMTD and U, the heat exchanger surface area required to reject Qc decreases (Equation 2). However, a trade-off occurs between increasing the shell-side mass flow rate (to enhance heat transfer and decrease the heat exchanger footprint) and increasing the shell-side pressure drop along with the incidental augmentation of the parasitic cooling load (Equation 4). As the shell-side mass flow rate increases, the increase in LMTD and decrease in required area plateaus while the additional parasitic losses grow exponentially. Consequently, increasing the shell-side mass flow rate beyond 200 kg/s for fields above the 500 m^2 heat exchanger surface area cut-off point cannot bring them below this point. Therefore, South Sean is still made the best choice for further analysis in Section 5 when including heat exchanger size as a measure of practicality in addition to net power output. Notably, the shell-side mass flow rate used to calculate the parasitic load in Section 5 was chosen as double that of the optimised thermosiphon-generated mass flow rate.

6.2.3 Geological uncertainty

The individual reservoir geology of each gas field evaluated for CPG power production was initially discounted when screening for the best-case target field in Section 4. In doing so, the minimum requirements for constructing a thermodynamic cycle and estimating power generation were solely met with the reservoir temperature and pressure, all the while easing the data collection process. In the subsequent analysis of the chosen target field, South Sean, the reservoir permeability was assumed to be perfectly homogenous and of a uniform thickness. This allowed the frictional pressure drop in the reservoir to be simply calculated

using Darcy's law (Equation 12). However, a range of geological uncertainties remain with the potential to adversely affect power generation. As highlighted in Section 1, for example, the stratigraphic positioning of layers of varying permeability within a reservoir influences CO_2 flow from the injection well to the production well. Specifically, the produced CO_2 mass fraction, the migration pathway, and the frictional pressure drop can all be affected.

The reservoir architecture of the South Sean field is somewhat complex. In brief, the gas trap is fault-bounded and dip closed, with the Leman Sandstone (Rotliegend Group) reservoir rock resting unconformably upon Carboniferous strata. The Rotliegend Group was deposited under continental desert conditions and aeolian facies in the form of cross-bedded dunes are dominant. The sands of these dunes are fine to medium-grained, clean, well sorted, and have excellent permeability. At the base and upper parts of the sequence, wadi, sabkha, and lacustrine deposits occur which, although thin, have significantly lower permeability (Hillier, 2003). The reservoir varies in thickness from 73 to 82 m (Botman and van Lier, 2020).

The uncertainty associated with variations in reservoir geology when estimating CPG power production can be reduced by making use of gas production data. Peak gas flow rate data are indicative of what the existing wells might be capable of achieving in a CPG scenario. South Sean operated under a 'peak shaver' contract before entering a blowdown phase from 2011. Over the course of this contract, gas was produced at rates of up to 600 mmscfd for a few days per year to match elevated demand (Botman and van Lier, 2020). Across 7 production wells (Hillier, 2003), 600 mmscfd is converted to kg/s CO_2 for one well:

600/7 = 85.7 mmscfd
85,700,000/86400 = 991.9 scf/s
991.9*0.0283 (m^3-ft^3) = 28.1 m^3/s (ISA: 1atm, 60F)
28.1*(273.15/288.71) = 26.6 Nm^3/s (0°C)
By ideal gas law, molar volume at 0°C is 22.41 $m^3/kmol$ and mass is 44.01 kg/kmol
26.6 m^3/s * (1 kmol/22.41 m^3) * 44.01 kg/kmol = 52.2 kg/s

Considering the similar dynamic viscosities of CH_4 and CO_2 at the South Sean reservoir temperature and pressure (1E-05 (Wischnewski, 2022) and 5E-05 Pa s, respectively), with 52.2 kg/s can be compared with the results presented in Table 4. This conversion from peak gas production rate to CO_2 mass flow rate suggests the base case CO_2 mass flow rate is

achievable. However, the higher mass flow rates needed to optimise power generation in the 0.28 and 0.41 m well diameter cases are less certain. Importantly, the pressure drive may be significantly different from the gas production case to the CPG scenario and so this conversion is only a rough approximation.

6.3 General findings and recommendations

The purpose of this section is to review the findings of this study and provide recommendations for future work. First, power generation estimates are compared with some of those published in the literature and the power-saving benefit of offshore CPG is highlighted. Second, insights into CPG exploration are offered through scrutinising the process of selecting a target field. Third, recommendations are offered to build upon the findings of this study.

Looking at the literature, studies have examined the effects of many different variables on CPG power production. Variables may relate to the reservoir, wells, and surface plant, such as those listed in Table 1. Moreover, the method used to estimate power production depends on the desired level of confidence in that estimation. For these reasons, the design specific to any given CPG study must be carefully considered before power production values can be compared with those of another study. The direct CPG cycle design presented in this study is adapted from (Adams *et al*., 2014). In the 2014 CPG study, power production estimates are made for a range of varying reservoir conditions. Thus, power production estimates for the reservoir conditions most closely aligned with the South Sean reservoir can be compared to the estimates of this study.

Differences in design between each of the studies are now accounted for. First, as detailed in Section 6.2.1, a single effective density value is conservatively assumed throughout each well in this study to determine how the CO_2 thermodynamic state changes across the wells. On the other hand, (Adams *et al*., 2014) simulates wellbore flow by making use of EES. As a result, estimated power production is expected to be lower in this study, all else being equal.

Another key difference between the CPG system designs of (Adams *et al*., 2014) and this study pertains to the type of turbomachinery used to generate power in the surface plant. A sCO_2 turbine is used in this study, meaning the CO_2 fluid is only expanded so much that it remains in the supercritical phase. By contrast, (Adams *et al*., 2014) employs a multiphase turbine, whereby the CO_2 fluid is expanded below the critical point and into the two-phase region. Although less expansion equates to less work done by the sCO_2 turbine, it avoids an inherent complication of operating multiphase turbines; liquid drop out during the expansion can cause the blades to become impinged, potentially halting power production altogether. Overall, this difference in study design further increases the expected margin between the direct CPG power production estimates of (Adams *et al*., 2014) and this study.

However, a third important difference exists between the two study's designs, again relating to the project. Since the gas fields examined for their CPG electricity generation potential in this study are located offshore, seawater cooling can be used. Many existing CPG studies, including (Adams *et al*., 2014), are based on onshore systems. In onshore systems, evaporative cooling operates by passing large volumes of air through cooling towers to reject heat at the surface, requiring significant parasitic cooling fan loads. Such cooling towers have a large footprint that is unfeasible on a congested offshore structure. Conversely, a seawater-based shell and tube heat exchanger is more compact and provides a more efficient cooling medium than air. This type of cooling system is often already installed on many platforms for applications such as gas cooling associated with compression as a fundamental processing step to meet export pipeline specifications. Because of the reduced parasitic cooling load that offshore systems benefit from, power production estimates may be re-balanced to some extent when considering all three study design differences at once.

The power production estimates from each study are now compared. The supplementary information to (Adams *et al*., 2014) contains a series of plots for the power output per production-injection pair for different CPG configurations. Table 5 shows the reservoir conditions for the most similar case to South Sean, along with South Sean itself. Well conditions are the same for both studies (0.41 m diameters and 707 m spacings).

For an unpumped direct (onshore) CPG system, (Adams *et al*., 2014) estimates that 1.1 MWe can be produced under the reservoir conditions specified in Table 5. This value is double that of the estimate for South Sean (0.55 MWe, Table 4). Although the South Sean reservoir is

slightly shallower and cooler, which decreases the net power output of the CPG system, it has a higher transmissivity compared with the reservoir case selected from (Adams *et al*., 2014). This significant discrepancy in net power generation can be accounted for, in part, by considering two of the outlined differences in study design. To demonstrate this, using the wells solution as described in Section 6.2.1, in addition to using a two-phase turbine, increases the turbine power output of the South Sean frictionless case (Section 4) two-fold. This calculation is set out in the appendix where the CO_2 fluid is expanded to 6.5 MPa in the turbine.

	Direct CPG system	
Reservoir variable	(Adams *et al.*, 2014)	South Sean
Depth (km)	2.50	2.38
Temperature (°C)	102.5	94.4
Thickness (m)	305	77.7
Permeability (mD)	100	600
Transmissivity (mD-m)	30,500	46,620

Table 5: Reservoir variables of the South Sean CPG system and a direct CPG system published in the literature (Adams et al., 2014)

Overall, this cross-study comparison suggests that the power generation estimates presented in Sections 4 and 5 are relatively conservative. While the estimates of (Adams *et al*., 2014) and similar studies may be more comprehensive in some regards, the methodology used in this study distinctly allows power generation estimates to be made for a large group of offshore gas fields in a consistent and more manageable way.

Importantly, the previously described difference in net power generation estimates of (Adams *et al.*, 2014) and this study effectively masks the power-saving benefit of offshore CPG. This benefit is now highlighted by comparing the parasitic load values calculated in this study to the values achievable by equivalent onshore cooling systems. Implications of employing seawater cooling systems when screening offshore prospects for direct CPG potential are then discussed.

To quantify the reduction in parasitic load achieved by a shell and tube heat exchanger, the cooling tower parasitic load equation used by (Adams *et al*., 2014) is applied to the South Sean frictionless case from Section 4. In brief, the cooling tower parasitic load is found by multiplying the rate of heat extraction by the parasitic fraction. The parasitic fraction is the range temperature divided by the sum of the range and the approach temperature, where the range is the difference between the inlet and outlet temperatures of CO_2 passing through the cooling tower. This calculation is set out in the appendix. For the South Sean frictionless case, just 21 kWe is required to pump seawater around the shell-side of the heat exchanger to sufficiently cool the CO_2 fluid for re-injection. By contrast, the onshore cooling tower parasitic load amounts to 162 kWe. In this case, net power generation is around 40% higher for the offshore system (power generated by the turbine remains the same). For reservoirs of increasing depths, the difference in parasitic cooling load for onshore and offshore systems increases further. For example, the Boulton field reservoir reaches a depth of 3.8 km (Conway and Valvatne, 2003), making it the deepest reservoir considered for CPG in Section 4. In the offshore case for Boulton, around 10 kWe is required to pump seawater around the shell-side of the heat exchanger. This is slightly less than South Sean (21 kWe) since the pressure drop on the shell-side is lower on account of a decrease in velocity (the heat exchanger size is greater while the mass flow rate remains the same). Conversely, around 650 kWe is required to power fans in a cooling tower in the Boulton 'onshore case' since this parasitic load is directly proportional to reservoir depth.

Equation 5 states that net power generated by an unpumped CPG system is equal to the difference between power generated by the turbine and the parasitic cooling load. As set out above, the parasitic load for pumping seawater is minimal regardless of reservoir depth. Consequently, net power generation for offshore systems strongly depends on how much power is generated by the turbine. Power generated by the turbine is a function of both the temperature and the pressure of the reservoir from which the CO_2 fluid is extracted. The hydrostatic reservoir pressure increases with depth and deeper reservoirs tend to be of higher temperatures (some variance occurs depending on geothermal gradient). Therefore, when solely aiming to maximise net power generation, fields with the deepest reservoirs make the best choice for offshore direct CPG. This point is reflected in Figures 6 and 7; all fields with an estimated net power generation of 500 kWe and above have reservoirs that are at least 3km deep. By contrast, the parasitic cooling load for onshore direct CPG systems increases significantly with reservoir depth. For this reason, direct CPG systems that can make use of

seawater cooling have higher net power outputs than their onshore counterparts, and this is particularly the case for systems with deeper reservoirs.

The South Sean field was selected as the most suitable field from which quantities (power) can be recovered by the project (the CPG system). Without including heat exchanger size as a practical constraint on the selection process, the field with the highest net power production might be assumed as the best choice. Such an assumption carries with it two potentially significant shortcomings. Firstly, an exceptionally large shell and tube heat exchanger would be required to sufficiently cool the CO_2 fluid for reinjection (Figure 7). The highest net power producing field via a frictionless CPG system (Tyne West) has a 3.6 km deep reservoir, requiring the CO_2 to be cooled in a 1.87 x 14 m heat exchanger containing over 3000 tubes. In addition to being impractical for integration with an existing gas platform, this heat exchanger would be costly to manufacture. A potential solution to the impractical aspect of exceedingly large shell and tube heat exchangers is to use a subsea cooler as an alternative. Set below the sea surface, this type of cooling system is constrained neither by weight nor size. The second shortcoming of simply choosing the highest net power producer as the target field again relates to the fact that this field's reservoir is amongst the deepest as a matter of course. The results presented in Table 4 indicate that the existing gas wells of the South Sean field are likely too small in diameter to enable a high thermosiphon-generated mass flow rate. Considering the South Sean reservoir has outstandingly high permeability compared to the reservoirs of all other fields assessed in Section 4, it is anticipated that the wells would need to be retrofitted in any case to produce moderate amounts of power (in the order of hundreds of kilowatts electric). For this reason, choosing a deeper reservoir further increases the upfront capital investments requisite to an up-and-running direct CPG system.

The South Sean field reservoir depth is close to the average depth of all 64 fields accounted for in this study. The estimated geothermal gradient from the near surface (assumed as 11 °C) to reservoir is the highest of any field at 35.1 °C km^{-1}. With a high geothermal gradient, the specific enthalpy of CO_2 in the reservoir is comparatively higher than field with reservoirs of similar depths. This is what makes South Sean the highest net power producer in a frictionless system when including heat exchanger size as a practical constraint. Were reservoir thickness and permeability also considered in the process of selecting a target field, the best choice in terms of power generation potential and practicality would still be South Sean. With a moderate reservoir thickness and high permeability, the ability of CO_2 to flow

through the South Sean reservoir (transmissivity) is high when compared to the remaining top 9 prospects (Figure 8). Reservoir transmissivity of each of the top 10 prospects was calculated as a check to ensure the selection of South Sean as the target field. Nevertheless, any future studies aiming to select the best offshore CPG prospect may have to take transmissivity into account as a first-order control (particularly if the best choice in a frictionless system has low transmissivity).

Further recommendations are now offered to build upon the findings of this study. The production status of each gas field can be included as a constraining factor on the target field selection process. Including this factor when evaluating offshore direct CPG prospects is an important step towards realising the real-life application of CPG. Production status relates to when, where, and how gas is being or has been produced from a field. An abandoned field such as Juliet (Figure 8), for example, may be less suitable for establishing a CPG system in both practical and economic terms than a currently producing field. Opting for a currently producing field can avoid unnecessary decommissioning costs and make for a smoother transition from gas to geothermal power production. Where gas is produced from a reservoir, in other words the number and spacings of existing wells across a field, also affects the suitability of that field for CPG. If the distance between existing wells is too great, the net power output of a CPG system may be diminished due to increased frictional losses as CO_2 moves through the reservoir. If the existing wells are spaced too close together, the heat stored in the reservoir will deplete faster and power production may be sustained for a shorter time. New wells may have to be drilled if existing wells are not optimally spaced, driving up cost. Finally, how gas is being produced from a field can impact the suitability of that field for CPG. A field where CO_2-EGR is planned carries with it clear economic benefits for establishing a CPG system. Similarly, planned offshore carbon storage sites offer synergistic effects which may increase a field's suitability for CPG. Altogether, field production status is closely linked to UNFC criterion E, for which categories were defined to classify the gas fields as geothermal resources in Section 6.1. A comprehensive socio-economic analysis leading on from this study could accelerate a transition of CPG as a conceptual technology into the development phase.

7. Conclusion

Direct CPG power production has been estimated for 64 gas fields in the SNS. A few identified and simplifying assumptions were applied to demonstrate that moderate amounts of power (in the order of kilowatts electric) could be produced from 50 of these fields. Although impracticable by nature, these estimates are useful ranging values and act as a bridge to finding the most suitable field for CPG. The South Sean field was selected as the most suitable field for CPG as it produces the most power after applying heat exchanger size as a practical constraint. Power generation was then re-estimated for South Sean while considering the thermosiphon effect, as well as the frictional pressure drop that occurs as CO_2 moves through the wells and reservoir. An injection-production well doublet could produce 59 kWe with standard gas well diameters, and this value increases to 552 kWe when standard geothermal well diameters are used. The gas fields were then classified as geothermal resources in accordance with the United Nations Framework Classification for Resources and its specifications to geothermal resources. Classifying the gas fields in this way supports the normalisation of consistent reporting for geothermal resources under a universally acceptable scheme. UNFC classes are determined by categorising resources across three criteria, project feasibility, socio-economic viability, and geological knowledge. All 50 gas fields found to be net positive for direct CPG are classified as having ‘additional quantities in place’ and these quantities may become recoverable in the future. Although a comprehensive geological dataset exists for the gas fields, CPG is yet to be demonstrated as a working technology by a pilot project and no economic appraisal was carried out in this study.

The power generation estimates for the South Sean field are likely conservative as suggested by a follow-up cross-study comparison. Nonetheless, the results of this study highlight an important benefit unique to offshore CPG systems, that is, minimal parasitic cooling loads can be achieved using a seawater cooling system. As a result, offshore CPG systems have higher net power outputs than equivalent onshore systems. This difference becomes increasingly apparent as reservoir depth increases. It is recommended that a socio-economic analysis should be conducted in future work to evaluate the gas fields as geothermal resources with a higher level of confidence.

Overall, this research has demonstrated that near zero-carbon baseload power could be produced from natural gas fields in the Southern North Sea. CO_2-plume geothermal remains a possible way to extend the useful lifespan of these ageing fields. The integration of this technology with enhanced gas recovery and future carbon storage projects is likely essential to prove its economic viability.

8. References

Adams, B. and Kuehn, T., 2012. The complimentary nature of CO2-Plume Geothermal (CPG) energy production and electrical power demand. Proceedings of the ASME 2012 International Mechanical Engineering Congress & Exposition, November 9-15, 2012, Houston, Texas, USA, (IMECE2012-88704).

Adams, B., 2015. On the Power Performance and Integration of Carbon-dioxide Plume Geothermal (CPG) Electrical Energy Production. Ph.D. The University of Minnesota.

Adams, B., Fleming, R., Bielicki, J., Garapati, N. and Saar, M., 2021 (c). An Analysis of the Demonstration of a CO_2-based Thermosiphon at the SECARB Cranfield Site. Proceedings of the Forty-Sixth Workshop on Geothermal Reservoir Engineering, Stanford University, pp.68-77.

Adams, B., Kuehn, T., Bielicki, J., Randolph, J. and Saar, M., 2015. A comparison of electric power output of CO2 Plume Geothermal (CPG) and brine geothermal systems for varying reservoir conditions. Applied Energy, 140, pp.365-377.

Adams, B., Kuehn, T., Bielicki, J., Randolph, J. and Saar, M., 2014. On the importance of the thermosiphon effect in CPG (CO2 plume geothermal) power systems. Energy, 69, pp.409-418.

Adams, B., Ogland-Hand, J., M. Bielicki, J., Schädle, P. and Saar, M., 2021 (b). Estimating the Geothermal Electricity Generation Potential of Sedimentary Basins Using genGEO (The Generalizable GEOthermal Techno-Economic Simulator). Supplemental Information, S.55.

Adams, B., Vogler, D., Kuehn, T., Bielicki, J., Garapati, N. and Saar, M., 2021. Heat depletion in sedimentary basins and its effect on the design and electric power output of CO2 Plume Geothermal (CPG) systems. Renewable Energy, 172, pp.1393-1403.

Arain, H., 2021. Water Properties Calculator. [online] Hamzasreef.com. Available at: <https://www.hamzasreef.com/Contents/Calculators/WaterProperties.php> [Accessed 15 April 2022].

ASHRAE handbook, 2020. American Society of Heating, Refrigerating, and Air-Conditioning Engineers, Atlanta.

Barrufet, M., Bacquet, A. and Falcone, G., 2010. Analysis of the Storage Capacity for CO2 Sequestration of a Depleted Gas Condensate Reservoir and a Saline Aquifer. Journal of Canadian Petroleum Technology, 49(08), pp.23-31.

BEIS, 2016. Offshore Energy Strategic Environmental Assessment: Appendix 1 Environmental Baseline. [online] Assets.publishing.service.gov.uk. Available at: <https://assets.publishing.service.gov.uk/government/uploads/system/uploads/attachment_data/file/504559/OESEA3_A1f_Climate___Meteorology.pdf> [Accessed 2 June 2021].

BEIS, 2019. Digest of UK Energy Statistics (DUKES): natural gas. Department for Business, Energy & Industrial Strategy, 4, pp.64.

Borgia, A., Pruess, K., Kneafsey, T., Oldenburg, C. and Pan, L., 2012. Numerical simulation of salt precipitation in the fractures of a CO2-enhanced geothermal system. Geothermics, 44, pp.13-22.

BP plc, 2021. Statistical Review of World Energy 2021. [online] London: BP plc, p.11. Available at: <https://www.bp.com/content/dam/bp/business-sites/en/global/corporate/pdfs/energy-economics/statistical-review/bp-stats-review-2021-full-report.pdf> [Accessed 24 March 2021].

Brown, D., 2000. A hot dry rock geothermal energy concept utilizing supercritical CO_2 instead of water. Proceedings of the Twenty-Fifth Workshop on Geothermal Reservoir Engineering, Stanford University, pp.233-8.

Busby, J., 2013. Geothermal energy in sedimentary basins in the UK. Hydrogeology Journal, 22(1), pp.129-141.

Buscheck, T., Elliot, T., Celia, M., Chen, M., Sun, Y., Hao, Y., Lu, C., Wolery, T. and Aines, R., 2013. Integrated Geothermal-CO2 Reservoir Systems: Reducing Carbon Intensity through Sustainable Energy Production and Secure CO2 Storage. Energy Procedia, 37, pp.6587-6594.

Carbon-dioxide-properties.com, 2021. MegaWatSoft inc. CO2 Tables Calculator. [online] Available at: <https://www.carbon-dioxide-properties.com/co2tablesweb.aspx>.

Chen, Y., 2016. Pinch point analysis and design considerations of CO2 gas cooler for heat pump water heaters. International Journal of Refrigeration, 69, pp.136-146.

Conway, A. and Valvatne, C., 2003. The Boulton Field, Block 44/21a, UK North Sea. Geological Society, London, Memoirs, 20(1), pp.671-680.

Cornford, C. 1990. Source rocks and hydrocarbons of the North Sea. In: Glennie, K. W. (ed.) Introduction to the Petroleum Geology of the North Sea. Blackwell Scientific Publications, 294-361.

Cui, G., Pei, S., Rui, Z., Dou, B., Ning, F. and Wang, J., 2021. Whole process analysis of geothermal exploitation and power generation from a depleted high-temperature gas reservoir by recycling CO2. Energy, 217, p.119340.

Cui, G., Ren, S., Dou, B. and Ning, F., 2020. Geothermal energy exploitation from depleted high-temperature gas reservoirs by recycling CO2: The superiority and existing problems. Geoscience Frontiers, p.101078.

Cui, G., Ren, S., Rui, Z., Ezekiel, J., Zhang, L. and Wang, H., 2017. The influence of complicated fluid-rock interactions on the geothermal exploitation in the CO2 plume geothermal system. Applied Energy, 227, pp.49-63.

Cui, G., Zhang, L., Ren, B., Enechukwu, C., Liu, Y. and Ren, S., 2016. Geothermal exploitation from depleted high temperature gas reservoirs via recycling supercritical CO2: Heat mining rate and salt precipitation effects. Applied Energy, 183, pp.837-852.

Doornenbal, J., Kombrink, H., Bouroullec, R., Dalman, R., De Bruin, G., Geel, C., Houben, A., Jaarsma, B., Juez-Larré, J., Kortekaas, M., Mijnlieff, H., Nelskamp, S., Pharaoh, T., Ten Veen, J., Ter Borgh, M., Van Ojik, K., Verreussel, R., Verweij, J. and Vis, G., 2019. New insights on subsurface energy resources in the Southern North Sea Basin area. Geological Society, London, Special Publications, pp.SP494-2018-178.

Dredge, I. and Marsden, G., 2020. The Cygnus Field, Blocks 44/11a and 44/12a, UK North Sea. Geological Society, London, Memoirs, 52(1), pp.151-162.

ECE – Economic Commission for Europe (2013): United Nations Framework Classification for Fossil Energy and Mineral Reserves and Resources 2009 incorporating Specifications for its Application, ECE ENERGY SERIES No. 42, United Nations Publication, ISBN 978-92-1-117073-3.

Ezekiel, J., Ebigbo, A., Adams, B. and Saar, M., 2020. Combining natural gas recovery and CO2-based geothermal energy extraction for electric power generation. Applied Energy, 269, p.115012.

Falcone, G. (Chair), Antics, M., Baria, R., Bayrante, L., Conti, P., Grant, M., Hogarth, R., Juliusson, E., Mijnlieff, H., Nádor, A., Ussher, G., Young, K. (2016), Specifications for the application of the United Nations Framework Classification for Fossil Energy and Mineral Reserves and Resources 2009 (UNFC 2009) to Geothermal Energy Resources, Joint UNECE-IGA document, September 2016.

Falcone, G. and Conti, P., 2019. Regional and country-level assessments of geothermal energy potential based on UNFC principles. In: European Geothermal Congress.

Farshad, F. and Rieke, H., 2006. Surface Roughness Design Values for Modern Pipes. SPE Drilling & Completion, 21(03), pp.212-215.

Finger, J. and Blankenship, D., 2010. Handbook of Best Practices for Geothermal Drilling. International Energy Agency, Geothermal Implementing Agreement, Annex VII.

Fleming, M., Adams, B., Kuehn, T., Bielicki, J. and Saar, M., 2020. Increased Power Generation due to Exothermic Water Exsolution in CO2 Plume Geothermal (CPG) Power Plants. Geothermics, 88, p.101865.

Freifeld, B., Pan, L., Doughty, C., Zakem, S., Hart, K. and Hostler, S., 2016. Demonstration of Geothermal Energy Production Using Carbon Dioxide as a Working Fluid at the SECARB Cranfield Site, Cranfield, Mississippi. Proceedings of the Forty-First Workshop on Geothermal Reservoir Engineering, Stanford University, pp.218-232.

Friedli, H., Lötscher, H., Oeschger, H., Siegenthaler, U. and Stauffer, B., 1986. Ice core record of the 13C/12C ratio of atmospheric CO2 in the past two centuries. Nature, 324(6094), pp.237-238.

Ganjdanesh, R., Bryant, S., Orbach, R., Pope, G. and Sepehrnoori, K., 2013. Coupled Carbon Dioxide Sequestration and Energy Production From Geopressured/Geothermal Aquifers. SPE Journal, 19(02), pp.239-248.

Garapati, N., Randolph, J. and Saar, M., 2015. Brine displacement by CO2, energy extraction rates, and lifespan of a CO2-limited CO2-Plume Geothermal (CPG) system with a horizontal production well. Geothermics, 55, pp.182-194.

Garapati, N., Randolph, J., Valencia, J. and Saar, M., 2014. CO2-Plume Geothermal (CPG) Heat Extraction in Multi-layered Geologic Reservoirs. Energy Procedia, 63, pp.7631-7643.

Gast, R.E., Dusar, M., Breitkreuz, C., Gaupp, R., Schneider, J.W., Stemmerik, L., Geluk, M.C., Geißler, M., Kiersnowski, H., Glennie, K.W., Kabel, S. & Jones, N.S., 2010. Rotliegend. In: Doornenbal, J.C. and Stevenson, A.G. (editors): Petroleum Geological Atlas of the Southern Permian Basin Area. EAGE Publications b.v. (Houten): 101-121.

Gautier, D., 2003. Carboniferous-Rotliegend Total Petroleum System Description and Assessment Results Summary. U.S. Geological Survey Bulletin, (2211).

Glennie, K., 1998. Petroleum Geology of the North Sea. 4th ed. Hoboken: John Wiley & Sons, Ltd., pp.137-143.

Glennie, K.W., 2007. The Permo-Carboniferous Rotliegend of NW Europe. In: Wong, T.E. (Ed.): Proceedings of the XVth International Congress on Carboniferous and Permian Stratigraphy. Netherlands Academy of Arts and Sciences: 10-16.

Global CCS Institute, 2020. The global status of CCS: 2020. [online] Melbourne. Available at: <https://www.globalccsinstitute.com/wp-content/uploads/2021/03/Global-Status-of-CCS-Report-English.pdf>.

Gluyas, J. and Bagudu, U., 2020. The Endurance CO2 storage site, Blocks 42/25 and 43/21, UK North Sea. Geological Society, London, Memoirs, 52(1), pp.163-171.

Goffey, G. and Gluyas, J., 2020. United Kingdom Oil and Gas Fields: 50th Anniversary Commemorative Volume. 52nd ed. London: Geological Society.

Goudarzi, S., 2016. Modelling Enhanced Gas Recovery by CO2 Injection in Partially Depleted Reservoirs., Durham theses, Durham University. Available at Durham E-Theses Online: http://etheses.dur.ac.uk/11645/.

Gupta, N. and Vashistha, M., 2016. Carbon Dioxide Plume Geothermal (CPG) System-A New Approach for Enhancing Geothermal Energy Production and Deployment of CCUS on Large Scale in India. Energy Procedia, 90, pp.492-502.

Han, W., Stillman, G., Lu, M., Lu, C., McPherson, B. and Park, E., 2010. Evaluation of potential nonisothermal processes and heat transport during CO2 sequestration. Journal of Geophysical Research, 115(B7).

Harper, P., 2011. Assessment of the major hazard potential of carbon dioxide (CO2). [online] Hse.gov.uk. Available at: <https://www.hse.gov.uk/carboncapture/assets/docs/major-hazard-potential-carbon-dioxide.pdf> [Accessed 18 November 2021].

Hillier, A., 2003. The Sean North, Sean South and Sean East Fields, Block 49/25a, UK North Sea. Geological Society, London, Memoirs, 20(1), pp.825-833.

Hook, J., 2020. The Hewett Field satellites: Big Dotty, Little Dotty, Deborah, Della, Dawn and Delilah, Blocks 48/29a, 48/30a, UK North Sea. Geological Society, London, Memoirs, 52(1), pp.203-216.

Hughes, D., 2009. Carbon storage in depleted gas fields: Key challenges. Energy Procedia, 1(1), pp.3007-3014.

IEA, 2021a. Geothermal, IEA, Paris https://www.iea.org/reports/geothermal.

IEA, 2021b. Global Energy Review: CO2 Emissions in 2020, IEA, Paris https://www.iea.org/articles/global-energy-review-co2-emissions-in-2020.

IPCC, 2018. Global Warming of 1.5°C. [Masson-Delmotte, V., P. Zhai, H.O. Pörtner, D. Roberts, J. Skea, P.R. Shukla, A. Pirani, W. Moufouma-Okia, C. Péan, R. Pidcock, S. Connors, J.B.R. Matthews, Y. Chen, X. Zhou, M.I. Gomis, E. Lonnoy, T. Maycock, M. Tignor, and T. Waterfield (eds.)].

IRENA, 2020. Renewable capacity statistics 2020 International Renewable Energy Agency (IRENA), Abu Dhabi.

Kristensen, L., Hjuler, M., Frykman, P., Olivarius, M., Weibel, R., Nielsen, L. and Mathiesen, A., 2016. Pre-drilling assessments of average porosity and permeability in the geothermal reservoirs of the Danish area. Geothermal Energy, 4(1).

Lee, K., 1996. Classification of geothermal resources: an engineering approach. Twenty-First Workshop on Geothermal Reservoir Engineering, Stanford University (21), pp.22-24.

MacFarling Meure, C., Etheridge, D., Trudinger, C., Steele, P., Langenfelds, R., van Ommen, T., Smith, A. and Elkins, J. (2006). Law Dome CO2, CH4and N2O ice core records extended to 2000 years BP. Geophysical Research Letters, 33(14).

McDonnell, K., Molnár, L., Harty, M. and Murphy, F., 2020. Feasibility Study of Carbon Dioxide Plume Geothermal Systems in Germany−Utilising Carbon Dioxide for Energy. Energies, 13(10), p.2416.

Monaghan, A., Arsenikos, S., Quinn, M., Johnson, K., Vincent, C., Vane, C., Kim, A., Uguna, C., Hannis, S., Gent, C., Millward, D., Kearsey, T. and Williamson, J., 2017. Carboniferous petroleum systems around the Mid North Sea High, UK. Marine and Petroleum Geology, 88, pp.282-302.

Morris, D., Pinnegar, J., Maxwell, D., Dye, S., Fernand, L., Flatman, S., Williams, O. and Rogers, S., 2018. Over 10 million seawater temperature records for the United Kingdom Continental Shelf between 1880 and 2014 from 17 Cefas (United Kingdom government) marine data systems. Earth System Science Data, 10(1), pp.27-51.

Mortensen, J., 1978. Hot dry rock: a new geothermal energy source. Energy, 3(5), pp.639-644.

Nwachukwu, C., Barnett, Z. and Gluyas, J., 2020. The Breagh Field, Blocks 42/12a, 42/13a and 42/8a, UK North Sea. Geological Society, London, Memoirs, 52(1), pp.109-118.

Oil and Gas Authority, 2018. Gas-to-Wire: UK SNS & EIS. [online] London: Oil and Gas Authority. Available at: <https://www.ogauthority.co.uk/media/5049/oil-gas-gas-to-wire.pdf> [Accessed 15 April 2021].

Oil and Gas Authority, 2019. UK Oil and Gas: Reserves and Resources Report. London: OGA Oil and Gas Authority 2020.

Ouyang, L., 2011. New Correlations for Predicting the Density and Viscosity of Supercritical Carbon Dioxide Under Conditions Expected in Carbon Capture and Sequestration Operations. The Open Petroleum Engineering Journal, 5(1), pp.13-21.

Pan, L., Freifeld, B., Doughty, C., Zakem, S., Sheu, M., Cutright, B. and Terrall, T., 2014. Fully coupled wellbore-reservoir modeling of geothermal heat extraction using CO2 as the working fluid. Geothermics, 53, pp.100-113.

Patel, M., May, E. and Johns, M., 2016. High-fidelity reservoir simulations of enhanced gas recovery with supercritical CO2. Energy, 111, pp.548-559.

Pattison, J., 2021. LIR Resources. [online] Lir-resources.com. Available at: <http://www.lir-resources.com/Operations/SouthernNorthSea> [Accessed 10 September 2021].

Pruess, K., 2004. The TOUGH Codes--A Family of Simulation Tools for Multiphase Flow and Transport Processes in Permeable Media. Vadose Zone Journal, 3(3), pp.738-746.

Pruess, K., 2006. Enhanced geothermal systems (EGS) using CO2 as working fluid—A novel approach for generating renewable energy with simultaneous sequestration of carbon. Geothermics, 35(4), pp.351-367.

Randolph, J. and Saar, M., 2011. Combining geothermal energy capture with geologic carbon dioxide sequestration. Geophysical Research Letters, 38(10).

Randolph, J. and Saar, M., 2011b. Coupling carbon dioxide sequestration with geothermal energy capture in naturally permeable, porous geologic formations: Implications for CO2 sequestration. Energy Procedia, 4, pp.2206-2213.

Randolph, J., Adams, B., Kuehn, T. and Saar, M., 2012. Wellbore heat transfer in CO2-based geothermal systems. in Geothermal Resources Council Annual Meeting 2012, GRC 2012 - Geothermal: Reliable, Renewable, Global. Transactions - Geothermal Resources Council, vol. 36 1, pp. 549-554.

Rybach, L., 2015. Classification of geothermal resources by potential. Geothermal Energy Science, 3(1), pp.13-17.

Sharqawy, M., Lienhard, J. and Zubair, S., 2010. Thermophysical properties of seawater: a review of existing correlations and data. Desalination and Water Treatment, 16(1-3), pp.354-380.

Smith, R., 2005. Chemical Process Design and Integration. 2nd ed. Chichester: John Wiley & Sons Ltd, pp. 661-666.

Span, R. and Wagner, W., 1996. A New Equation of State for Carbon Dioxide Covering the Fluid Region from the Triple-Point Temperature to 1100 K at Pressures up to 800 MPa. Journal of Physical and Chemical Reference Data, 25(6), pp.1509-1596.

Span, R., Wagner, W. Equations of State for Technical Applications, 2003. Simultaneously Optimized Functional Forms for Nonpolar and Polar Fluids. International Journal of Thermophysics 24, 1–39. https://doi.org/10.1023/A:1022390430888

Ueda, A., Kato, K., Ohsumi, T., Kaieda, H., Ito, H., Savage, D., Metcalfe, R. and Takase, H., 2005. Experimental and Theoretical Studies on CO2 Sequestration into Geothermal Fields. Proceedings World Geothermal Congress, April 24–29, Antalya, Turkey.

Underhill, J., 2003. The tectonic and stratigraphic framework of the United Kingdom's oil and gas fields. Geological Society, London, Memoirs, 20(1), pp.17-59.

van Wees, J., Stephenson, R., Ziegler, P., Bayer, U., McCann, T., Dadlez, R., Gaupp, R., Narkiewicz, M., Bitzer, F. and Scheck, M., 2000. On the origin of the Southern Permian Basin, Central Europe. Marine and Petroleum Geology, 17(1), pp.43-59.

Welch, P. and Boyle, P., 2009. New turbines to Enable Efficient Geothermal Power Plants. GRC Transactions, Vol. 33, 2009. [online] Energent Corporation. Available at: <http://www.energent.net/documents/Geothermal_Resources_Council_2009_Paper.pdf> [Accessed 12 May 2021].

Wood, I., 2014. UKCS Maximising Recovery Review: Final Report.

Xu, T., Feng, G. and Shi, Y., 2014. On fluid–rock chemical interaction in CO2-based geothermal systems. Journal of Geochemical Exploration, 144, pp.179-193.

Xu, T., Zhu, H., Feng, G., Yuan, Y. and Tian, H., 2017. On Fluid and Thermal Dynamics in a Heterogeneous CO2 Plume Geothermal Reservoir. Geofluids, 2017, pp.1-12.

Zhang, L., Li, X., Zhang, Y., Cui, G., Tan, C. and Ren, S., 2017. CO 2 injection for geothermal development associated with EGR and geological storage in depleted high-temperature gas reservoirs. Energy, 123, pp.139-148.

9. Appendix 1

Appendix 1 consists of supplementary material intended to be used in conjunction with Appendix 2. Appendix 2 contains all the data and calculations implemented in this research. It is an excel file arranged by sheets that correspond to different sections within the thesis. The first sheet, 'Discounted fields', contains a list of SNS gas fields that have not been considered for their CPG power generation potential (this omittance is discussed in Section 3.4).

Fields with sufficient reservoir data are tested for their power generation performance in Section 4, all in the same way. This process is set out in the second excel sheet named 'Selecting a target field'; The thermodynamic properties of CO_2 at state 3 in a CPG cycle (see Figure 5 for reference) were initially filled in for each field as shown in the rows on the left-hand side of this sheet, under the heading 'State 3: production sandface'. Moving from left to right across the sheet, state 4 was then derived from state 3. This was done by calculating the change in enthalpy from state 3 to state 4 (column J) and hence the change in pressure from state 3 to 4, giving a pressure value at state 4 (column K). Temperature, density, and enthalpy at state 4 were then found from the known pressure value, under the assumption that entropy remains constant from state 3 to 4. Since entropy also remains constant through to state 5, and pressure is set to 7.5 MPa so that CO_2 remains in the supercritical phase, the temperature, density, and enthalpy were deduced in the same way for state 5. Equation 1 was then applied in column T to find the power produced by the turbine for each field in a direct frictionless CPG system. The next step taken towards finding the net power produced by the system (Equation 5) was to calculate the parasitic loss from pumping seawater through a heat exchanger at the surface in order to cool the CO_2 fluid prior to re-injection. The process of selecting an approach temperature for each field has been set out on the right-hand side of the sheet. The highlighted values were copied to column Z and the temperature of CO_2 in column Y was found from these values by using the known seawater temperature. Since pressure is constant from states 5 to 1, and the temperature has been calculated, the density, enthalpy, and entropy can be deduced for state 1.

The values presented in columns AB and AC within the sheet, 'Selecting a target field', have been copied from the third sheet in Appendix 2, titled 'Cooling calculations'. Equations 2, 3,

and 4 are applied in rows 46, 8, and 75 of the ‘cooling calculations’ sheet, respectively. The overall heat transfer coefficient (used in Equation 2) is shown in row 73 and the shellside pressure drop is shown in row 71 (used in equation 4). Both the overall heat transfer coefficient and the shellside pressure drop were found using a set of simplifying relations as described in Appendix C of (Smith, 2005). These relations are given on the left-hand side of the sheet, adjacent to the cells in which they have been applied. They are based on the heat exchanger design and the thermodynamic properties of CO_2 and seawater flowing through the heat exchanger, which are presented in rows 10 to 43.

Net power produced by a direct CPG system configured to each field is given in column AJ in the ‘selecting a target field’ sheet, as well as column L in the ‘Cooling summary’ sheet. The ‘Cooling summary’ sheet contains only the primary values obtained from ‘Cooling calculations’ that have been applied in Equations 2, 3, and 4, along with net power production values from the sheet ‘Selecting a target field’.

The fifth sheet, titled ‘(Section 5) South Sean’, demonstrates how CPG power production was re-estimated for the South Sean field while taking frictional pressure losses into account. The same process has been carried out for the South Sean CPG system configured with 3 different well diameters, which are colour coded. The 4 rows on the left-hand side (above the graphs) show the reservoir, well, and CO_2 properties required to determine frictional losses. The constant values forming part of the pressure loss Equations (11 and 12) were calculated in columns L and M from these properties. The constant values were then employed in the 3 column groups on the right-hand side for each well diameter to show how pressure losses increase with mass flow rate. The rows highlighted in yellow indicate the maximum power that can be produced from a thermosiphon-generated pressure difference of 2.41 MPa.

‘Study comparison demonstrations’ is the final sheet presented in Appendix 2. This sheet illustrates points made in Sections 6.2.1 and 6.3. In Section 6.2.1, the assumption of assigning effective density values to each well in a CPG system is scrutinised. It was determined that the thermosiphon-generated pressure difference and the net power output of the CPG system are underestimated by using the effective density and that this error can be reduced by modelling the change in pressure as CO_2 moves along each well. Models of the injection and production wells are set out in this sheet. Each row represents a 100 m increment along each well, and the change in pressure was calculated recursively as stated in the text. The

highlighted values beneath the production well model are equivalent to state 4 in the South Sean CPG system. The same values were then used on the right-hand side of the sheet under the heading, ‘Integrating the well demonstration method with a two-phase turbine in a 100 kg/s frictionless scenario’. This table relates to Section 6.3, where the wells solution described above is implemented in a CPG system that uses a two-phase turbine. The turbine power output is presented below the table, which is compared to the results of a CPG study in the literature.